dti

DESIGN & MANUFACTURE OF RADAR ABSORBING WIND TURBINE BLADES – FINAL REPORT

CONTRACT NUMBER: W/44/00636/00/REP

URN NUMBER: 05/1409

The DTI drives our ambition of 'prosperity for all' by working to create the best environment for business success in the UK.
We help people and companies become more productive by promoting enterprise, innovation and creativity.

We champion UK business at home and abroad. We invest heavily in world-class science and technology. We protect the rights of working people and consumers. And we stand up for fair and open markets in the UK, Europe and the world.

DESIGN & MANUFACTURE OF RADAR ABSORBING WIND TURBINE BLADES – FINAL REPORT

CONTRACT NUMBER:
W/44/00636/00/REP
URN NUMBER: 05/1409

Contractor QinetiQ

Prepared by Dr Stephen G Appleton

February 2005

The work described in this report was carried out under contract as part of the DTI Technology Programme: New and Renewable Energy, which is managed by Future Energy Solutions. The views and judgements expressed in this report are those of the contractor and do not necessarily reflect those of the DTI or Future Energy Solutions.

First published 2005

EXECUTIVE SUMMARY

This report describes the results of the DTI-supported project Design & Manufacture of Radar Absorbent Wind Turbine Blades; a collaborative project between QinetiQ Ltd. and NOI (Scotland) Ltd. The aims of the project were threefold:

- to understand, through predictive modelling, the contribution made by the blade to the radar cross section (RCS) of a complete turbine
- to gain confidence that the turbine RCS can feasibly be reduced to appropriate levels by the use of radar absorbent material (RAM)
- to demonstrate that RAM variants of the blade materials can be manufactured, by the introduction of stealth technology within the current composite sections, with minimal structural impact

Research performed

The activities that have been performed to achieve the overall project aims include:

- The RCS of a turbine (comprising a generic tower and nacelle plus a set of 34m blades made by NOI) has been predicted at frequencies at which representative air traffic control (ATC), weather and marine navigation radar systems operate. A range of turbine yaw and blade pitch combinations have been considered, but emphasis has been placed on the configurations that give maximum Doppler returns to ATC radar. Predictions were performed using the SPECTRE software, a fully validated RCS code developed by QinetiQ, which was modified to include predictions of rotating blades. Computer aided drawing (CAD) depictions of the NOI blade were created from engineering drawings and the CAD was meshed in such a way that the radar reflectivity of different regions of the blade could be specified.

- The various material compositions that exist on the NOI blade were studied, and methods by which RAM could be introduced to each region were identified. Materials present include solid glass fibre-reinforced epoxy (GRE) and GRE-skinned foam sandwich panels of a range of thicknesses. Materials samples were supplied by NOI, and their microwave properties were measured and then used as input to RAM design codes that have been developed by QinetiQ and validated over many years. RAM designs have been sought that minimise the risk of any reduction in structural integrity of the blade. This was seen as a key issue by DTI, and was the reason for the project review point after Stage 1.

- RCS predictions were repeated for a blade having RAM over its surface. Predicted reflectivity (derived during the RAM design activity) for each different RAM type was attributed to the appropriate positions along the blade, taking into account the variation of reflectivity with polarisation and angle of incidence. The benefits of applying RAM to the nacelle and tower were also assessed.

- The NEMESiS propagation model was run for two representative geographical locations, to gain an understanding of the detectability of a turbine by each radar type. This was undertaken for standard blades and for RAM blades, and for the cases of metal and RAM-treated tower and nacelle.

Results & conclusions

The work performed has given QinetiQ and NOI an excellent understanding of the opportunities for creating stealthy blades. The key outcomes were as follows:

- It is possible to modify the solid GRE and GRE/foam sandwich panel materials used in the NOI 34m blade to create RAM, through the replacement of a single layer of glass cloth by an electromagnetically modified version of the same material. Absorption in the range 20dB to 30dB (i.e. reflected power is < 1% of incident power) can be readily achieved, even at the low frequencies (and hence large wavelengths) used by ATC radars. Performance of >25dB was achieved for most materials, though such fine-tuning for every material type was not considered necessary, as the main aim was to show proof-of-concept. This RAM approach is known to result in little or no degradation in the structural integrity of the blade materials, is compatible with the manufacturing processes used by NOI (and by most other blade manufacturers) and can be achieved at acceptable cost.

- RCS calculations show that treatment of the blade surfaces with 25dB RAM leads to a comparable reduction in the peak RCS. The background RCS level (i.e. between peak flashes caused by the leading and trailing edges) remains unaltered for a metal tower and nacelle, whose large static RCS dominate. If the entire turbine is treated with RAM, then the background RCS is reduced and interactions between the blades and turbine are also suppressed. It appears feasible to reduce the median RCS to well below 0dBsm, a threshold value typical of that used by ATC radar operators to discriminate between false alarms and moving aircraft.

- The impact of RCS reduction on the detection of the turbine by radar systems was calculated for cases where the whole turbine was treated with RAM. Although a modest decrease in the maximum detection range was found for weather radar (as is expected for such relatively powerful systems), much more significant reductions were predicted for ATC and marine radars. In the case of a turbine situated at the Hare Hill wind farm site in Scotland, it was predicted that the RAM-treated turbine would be undetected by the ATC radar at nearby Prestwick airport for the majority of turbine orientations.

Recommendations

In summary, the study has shown that it is possible to modify all materials regions of the NOI 34m blade to create RAM, and that this can be done with little or no degradation in structural properties. The predicted benefits in terms of reduced detection by non-Doppler radar and ATC radars are seen to be extremely encouraging.

However, predictive models can never fully represent reality, and there are factors that are difficult to accurately model, such as blade twist and bend. In light of this, it is recommended that a full practical demonstration of a stealthy turbine should be performed. All stakeholders (developers, manufacturers and planning objectors) will then be able to quantify the benefits of RCS reduction through the use of RAM.

CONTENTS PAGE

This page is intentionally blank

1 INTRODUCTION

1.1 Background

1.1.1 There has been a steady increase in the number of installations and in the number of proposals for new wind farms, including both onshore and offshore sites. However, the size, movement and density of turbines in a typical wind farm result in the possibility of interference being caused to incident radar signals. Several different types of radar might be affected, including those used for weather monitoring, marine navigation aids and air traffic control (ATC). Consequently, there have been several occasions where planning applications for new wind farms have been rejected on the grounds that one or more radar systems would be adversely affected.

1.1.2 Previous research conducted by QinetiQ under DTI funding [1] quantified the level of interaction between radar signals and standard wind turbines. It was shown that rotating blades can, in some combinations of turbine orientation and blade angle, cause significant doppler returns to the illuminating radar, thereby creating confusion or distraction for radar operators. The sporadic nature of such high level blade 'flashes' (i.e. the radar will not be positioned to detect these high returns on every rotation) makes them difficult to filter within the radar software.

1.1.3 It is certainly advisable for the layout of turbines within a wind farm to be designed for minimal radar impact, and radar filters can be used to remove some unwanted signals. However, it is considered unlikely that such measures alone will totally negate radar interference and that further benefit can be gained by reducing the radar reflectivity of the turbines themselves.

1.1.4 Consequently this current project aims to study the feasibility and benefits of creating radar-absorbent wind turbine blades.

1.2 Aims of the project

1.2.1 The project was performed jointly by QinetiQ Ltd. and NOI Scotland Ltd., a blade manufacturer based in Fife. There were several aims of the project:

- Predict the Radar Cross Section (RCS) of a turbine comprising a generic tower and nacelle plus a set of 34m blades made by NOI. Predictions were to be made using the SPECTRE software, a fully validated RCS code developed by QinetiQ. RCS was to be predicted for a number of combinations of turbine orientations, blade pitches and radar types, but with a particular emphasis on ATC radar.

- Use this RCS data as input to simulations of radar systems of the types known to have been at the source of objections to wind farm sites. The

simulations were to be made using the NEMESiS propagation code, and would make use of radar parameters supplied by radar operators and/or documented in open literature publications.

- Repeat the RCS predictions and radar simulations for blades incorporating radar-absorbent materials of realistically achievable performance, and hence determine the effectiveness of such reduced RCS blades in minimising the impact on radar systems.

- Demonstrate that it is possible to produce RAM blades at acceptable cost, scale and quality, without compromising structural integrity. This was to begin with characterisation of the materials used in the current NOI blades, gaining an understanding of how the blades are manufactured and how they can be modified to include radar absorbent additives. RAM versions of the different materials used on the NOI Scotland blade were then to be designed by QinetiQ and flat panels were to be produced by NOI Scotland. Finally, after iteration of the RAM designs, blade sections were to be produced and validated.

1.3 Deviations from the project plan

1.3.1 It was originally intended that all RAM materials would be produced by NOI Scotland, by the same techniques that are used for blade manufacture. However, NOI Scotland ceased trading during the course of the project and were unable to commit effort to production of RAM panels or blade sections. It was agreed with the DTI that QinetiQ would produce RAM panels using nominally the same methods as NOI Scotland, and the project was extended to allow time for QinetiQ to perform these additional tasks.

2 RCS PREDICTIONS

2.1 The Spectre model

2.1.1 The RCS of the computer aided design (CAD) model of the turbine was calculated using QinetiQ's RCS prediction tool, 'Spectre'. Spectre was specifically developed to model the RCS of large, complex targets. The code has been operational for over ten years and has been thoroughly validated against measured data. During this time, it has been subject to continuous development to enhance its capabilities and computing efficiency.

2.1.2 Spectre is a high frequency code that simulates scattering using well-established, stable approximations. Reflections are modelled using a combination of physical and geometric optics. Diffraction effects are represented by an equivalent-current extension of the physical theory of diffraction, which produces accurate results on and off the Keller cone. These methods produce reliable, accurate predictions for well-defined bodies.

2.1.3 Spectre can simulate scattering from a wide range of absorbing materials, using look-up tables that can be generated from measurements or calculations. To simulate the effects of the environment, it includes a fully bistatic multipath model and allows the target to roll and pitch arbitrarily.

2.1.4 In order to allow for the blades on a wind turbine, Spectre was enhanced to model the effects of rotating features on the target. The modification allows the user to identify specific parts of the CAD model as rotating features. The geometry is then updated at every time step before the RCS is calculated.

2.2 Turbine CAD

2.2.1 In order to calculate the RCS of a turbine, a suitable three-dimensional CAD representation is required. The one used in this study was constructed by QinetiQ's CAD centre using blade profile and twist data supplied by NOI Scotland [2].

2.2.2 A finite element mesh was then applied to the CAD so that the mesh was within 1mm of the original surface. As a general rule, meshes need to be within 1/16 of a wavelength of the original surface in order to be sufficiently accurate for RCS prediction purposes. A tolerance of 1mm is therefore sufficiently accurate to model wavelengths down to 16mm (frequencies up to 18.75GHz).

2.2.3 The mesh that was produced from this process is illustrated in Figure 2-1. In this diagram, GRE is an abbreviation for glass reinforced epoxy and FS stands for foam sandwich. The blade girder was modelled as 15 mm GRE as this was expected to have similar scattering properties to the actual

material used. In addition to the materials visible in Figure 2-1, the model also contained a leading edge cap, also modelled as 15mm GRE.

2.2.4 This blade was then added to a generic turbine and hub arrangement of the kind illustrated in Figure 2-2. The properties of the tower and hub were chosen to be metallic (i.e. reflective to radar signals). The baseline turbine RCS was calculated using this model.

2.2.5 A second model was then defined, with the materials shown in Figure 2-1 replaced by low RCS alternatives. The 6-20 mm FS regions were attributed with the properties of FS RAM and the leading edge cap, girder and blade root were replaced with a GRE RAM. All RAM performance values were derived from predictions that were performed as a function of angle of incidence for each of the materials, at each of the three radar frequencies being studied (ATC 2.885 GHz, weather 5.625 GHz and marine navigation 9.1375 GHz).

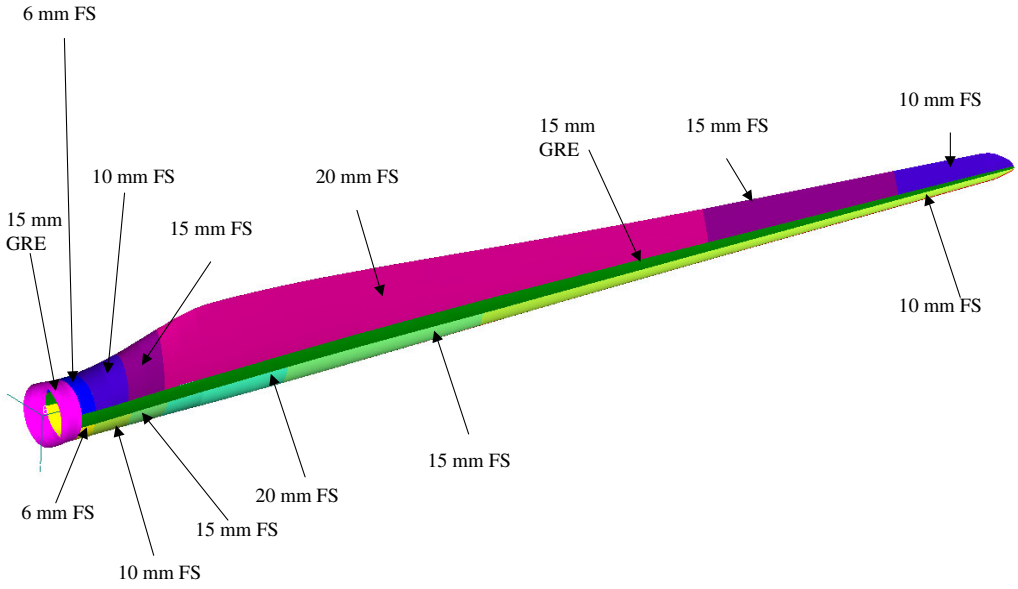

Figure 2-1 Blade CAD showing material regions

2.3 Calculations performed

2.3.1 The RCS of the two turbine variants was calculated for three different generic radars:

- A generic ATC radar, 2.885 GHz, horizontal polarisation;
- A weather radar operating at 5.625 GHz, vertical polarisation;
- A typical marine navigation radar operating at 9.1375 GHz horizontal polarisation.

For the purposes of these calculations, the relative location of the radar was defined in terms of the yaw angle of the turbine hub, where 0° yaw corresponds to the hub pointing towards the radar.

2.3.2 The highest level of Doppler shift in the return will occur when the blades are viewed leading-edge-on at 0° pitch and 90° yaw, as this is when the component of motion towards the radar is greatest and the blade is viewed edge-on (see Figure 2-3). This case was analysed for all of the radars listed above.

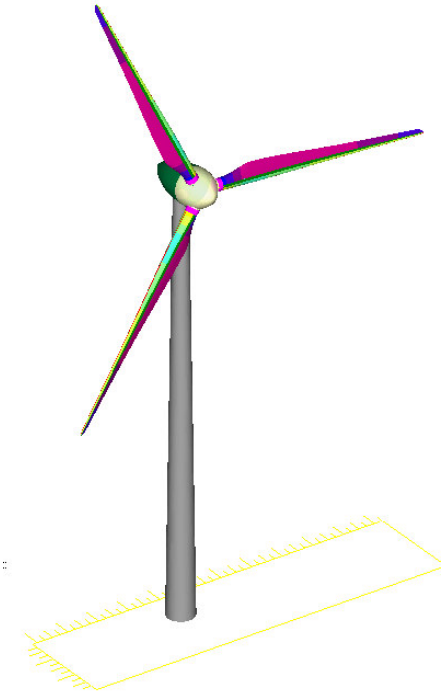

Figure 2-2 CAD of complete turbine

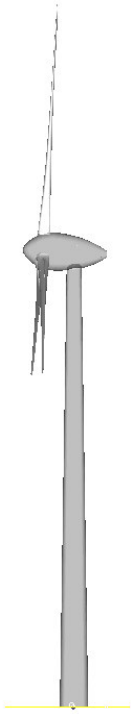

Figure 2-3 Blades oriented for maximum Doppler RCS

2.3.3 To investigate the effects of yaw angle, the RCS was also calculated for 0°, 30° and 60° yaw for the ATC radar. A typical radar system will have an unambiguous range of up to 150km. This corresponds to a maximum possible pulse-repetition frequency of 1kHz. If the blade tips are rotating at 100 m/s at a radius of 35m, this means that a 360° rotation of the blades will take approximately 2.2 seconds. This means that the blades can be expected to rotate approximately 0.16° in-between pulses. The Spectre calculation was deliberately over-sampled at 0.1° intervals of blade axis rotation.

2.3.4 In each case, the RCS was plotted as a function of blade rotation angle[1] and the median and peak values assessed. The amount of signal that passes through the blade surface and is scattered back from internal structures was accounted for by modifying the effective surface reflectivity of the blade, based on measurements made on a blade section (see Section 4.2 for details). This was not necessary for the metallic tower and nacelle, nor for the RAM-treated components, since these contain an integral reflective layer.

[1] This was chosen in preference to time as it is independent of blade speed.

2.4 ATC results

2.4.1 Un-treated turbine

2.4.1.1 The 0° yaw case is probably the least significant from a radar point of view, as there will be very little Doppler shift on the returns. As a result, they are likely to be filtered out by the radar. However, as can be seen from Figure 2-4, the RCS values are high in this case as the blades are presenting the maximum area to the radar and the tower and nacelle are also strongly scattering. The median RCS is 30dBsm.

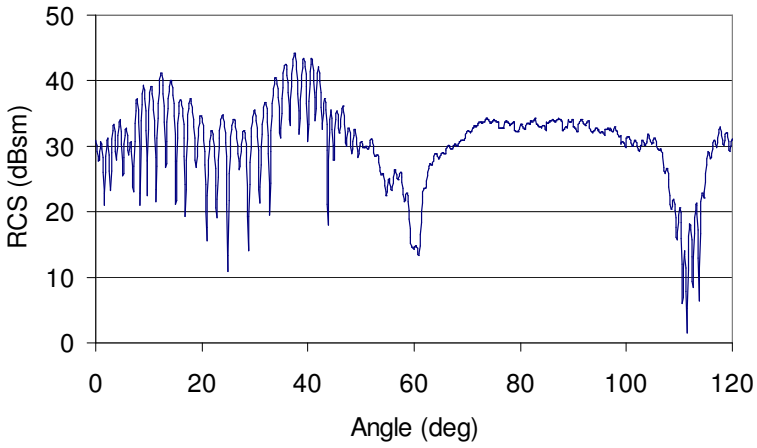

Figure 2-4 RCS of the original turbine at 0° yaw

2.4.1.2 In the 30° case, the maximum RCS occurs at 80.3°, but the RCS is relatively low elsewhere, as can be seen from Figure 2-5. The median RCS is 15dBsm. A similar pattern can be seen in the 60° case (Figure 2-6), where the median RCS is 13dBsm.

2.4.1.3 In the 90° case, the peak RCS occurs when the blade is near to the vertical. In reality, the leading edge is not perfectly straight, and hence there are several components to the peak, possibly corresponding to individual regions of straight blade or to interactions between the blade and the tower. The highest RCS levels are distributed over a small angular window near 26° angle of rotation, as seen in Figure 2-8. This RCS plot shows the 30dBsm leading edge flash, plus a smaller and more distributed trailing edge return near 85°. The median RCS level is 12dBsm.

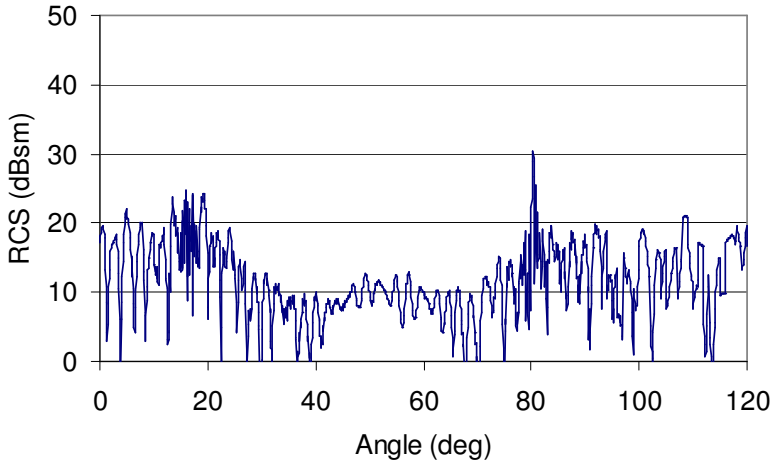

Figure 2-5 RCS of the original turbine at 30° yaw

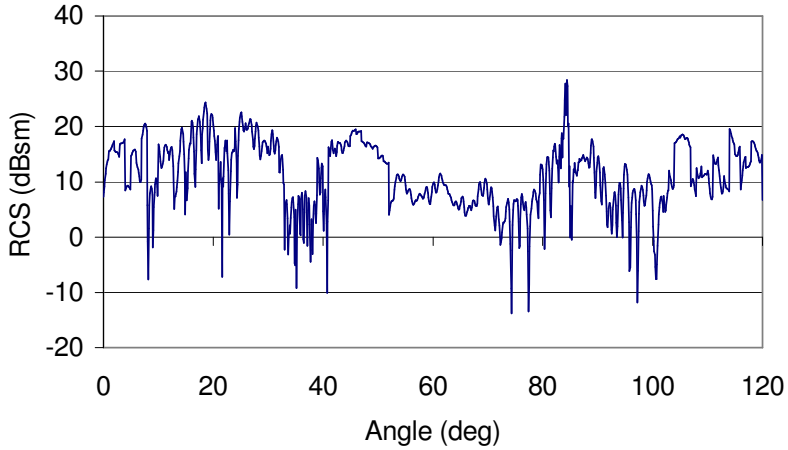

Figure 2-6 RCS of the original turbine at 60° yaw

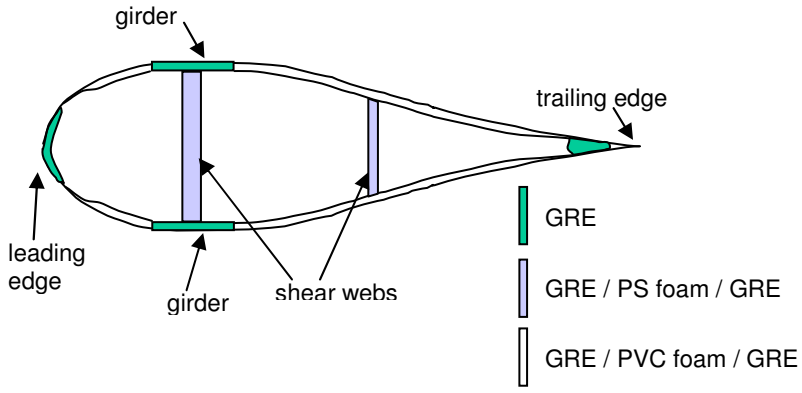

Figure 2-7 Schematic of blade construction

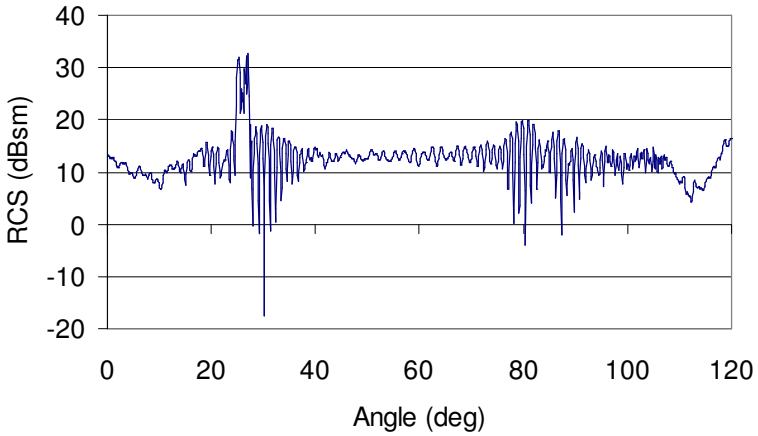

Figure 2-8 RCS of the original turbine at 90° yaw

2.4.2 RAM-treated turbine

2.4.2.1 Radar absorbing materials (with ~25dB absorption performance) were then added to the design, as described in Section 2.2, to differing degrees of RAM treatment:

- Blades only
- Tower & nacelle RAM + full blade RAM
- Tower & nacelle RAM + outer 33% of blade (full circumference treated)
- Tower & nacelle RAM + outer 67% of blade (full circumference treated)
- Tower & nacelle RAM + leading edge region of blade

The aim of predicting the latter 3 cases was to begin to gain an understanding of the likely treatment areas that will be required, so that the most cost-effective treatment scheme can be devised. The majority of calculations were for 90° yaw, as this is seen as the most problematic case for ATC radar, but the whole RAM turbine case was run for 0° yaw as well.

2.4.2.2 Blade only: The RCS at 90° yaw for the case where the blades only are treated is shown in Figures 2-9 (full 120° rotation) and 2-10 (detail of leading edge flash). As expected, the RAM has little effect on the median RCS since this is dominated by the contribution from the reflective metal tower and nacelle. The leading edge flash is reduced more significantly by the RAM blades, such that the peak is within variations in the background level (i.e. the level between the leading and trailing edge flashes). The peak RCS in this case is 17dBsm, compared to 31dBsm for the original turbine.

2.4.2.3 The effectiveness of the RAM can be confirmed through the use of hotspot plots. These colour an object according to the strength of the RCS returns from different parts. As can be seen from Figure 2-11, the RCS of the turbine with RAM blades only is now dominated by the RCS of the tower.

2.4.2.4 Whole turbine: The benefit of applying RAM to the tower and nacelle, as well as to the blades, is that the median *and* leading edge flash RCS levels are reduced, as demonstrated by Figures 2-12 and 2-13 respectively. The median RCS has been reduced from 12dBsm to -11dBsm and the leading edge flash is a maximum of 8dBsm and averages at -1dBsm. This is an extremely encouraging result, as the peak equivalent size of the turbine is reduced from >1000m^2 to less than 6m^2 at worse, **suggesting that a RAM treated turbine might no longer be identified by ATC radar as being a potential aircraft.**

2.4.2.5 Blade treatment study: The results from the study of different blade treatment areas are summarised in Figure 2-14. The tower and nacelle are RAM-treated, and the median RCS is relatively independent of the blade treatment scheme. Hence Figure 2-14 only shows the peak RCS. There is relatively little difference between these cases, although the full RAM blade performs best. Measurement trials using a real radar system would be necessary before a particular blade treatment scheme could be chosen with confidence.

2.4.2.6 The 0° yaw case showed a dramatic reduction in both median and peak RCS, though the residual RCS after RAM treatment is relatively large as seen in Figure 2-15. However, the zero Doppler component is large for this orientation and should be removed by a moving target indicator (MTI) filter.

2.4.2.7 The median and peak RCS values for all treatment cases are given in Table 2-1.

			Median RCS		Peak RCS	
			m^2	dBsm	m^2	dBsm
90° yaw	No RAM		18	13	1,202	31
	RAM blades		17	12	54	17
	RAM tower RAM nacelle	Blade leading edge	< 0.1	-11	18	13
		Outer 33% of blade	< 0.1	-10	12	11
		Outer 67% of blade	< 0.1	-10	9	10
	Whole turbine RAM		< 0.1	-11	6	8
0° yaw	No RAM		1,130	31	26,790	44
	Whole turbine RAM		54	17	344	25

Table 2-1 Summary of ATC RCS results

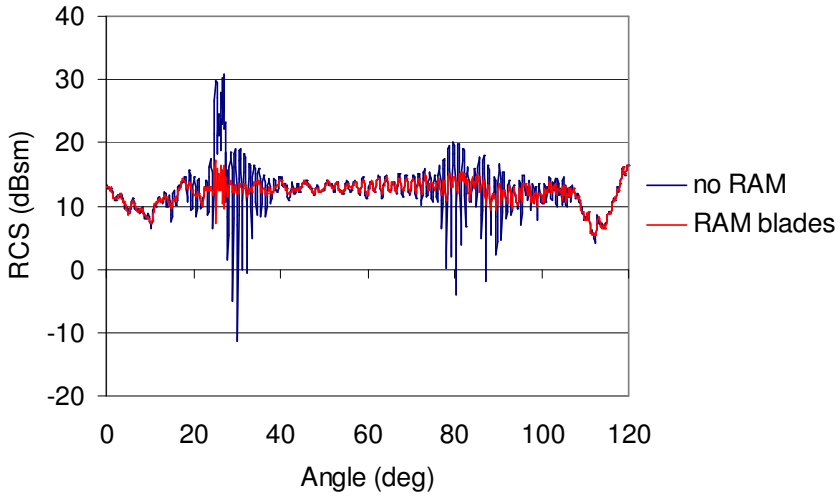

Figure 2-9 RCS for RAM blades only (90° yaw)

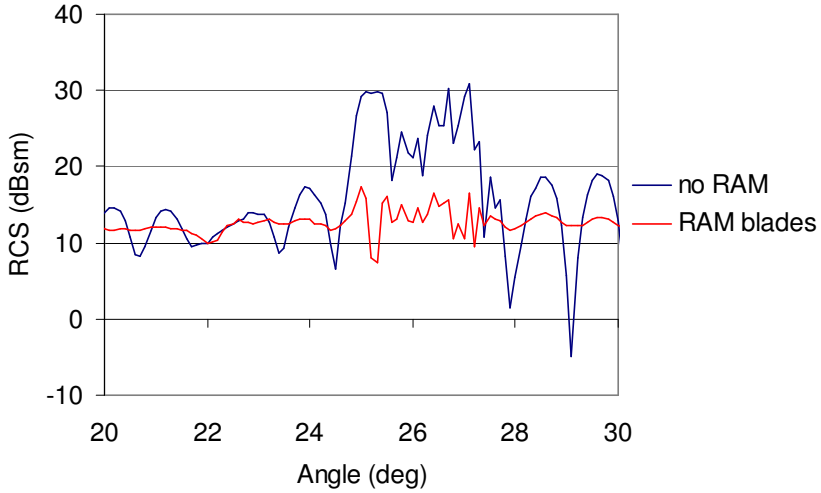

Figure 2-10 Leading edge flash RCS for RAM blades only (90° yaw)

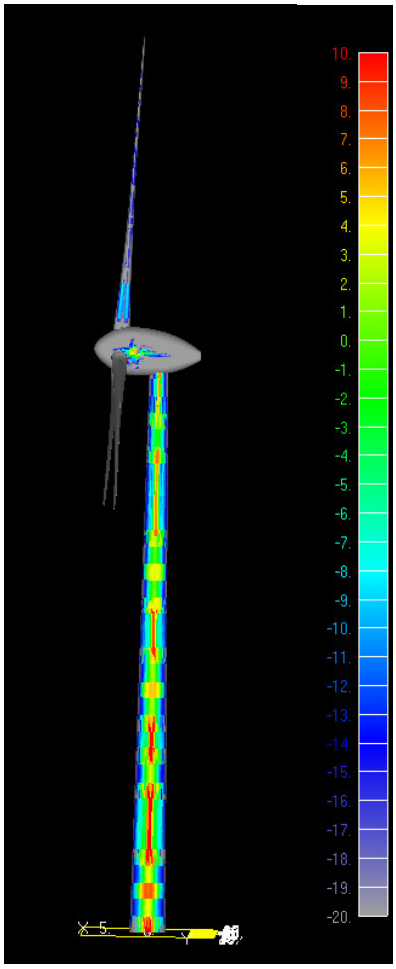

Figure 2-11 RCS hotspot plot of turbine with RAM blades (tower RCS dominates)

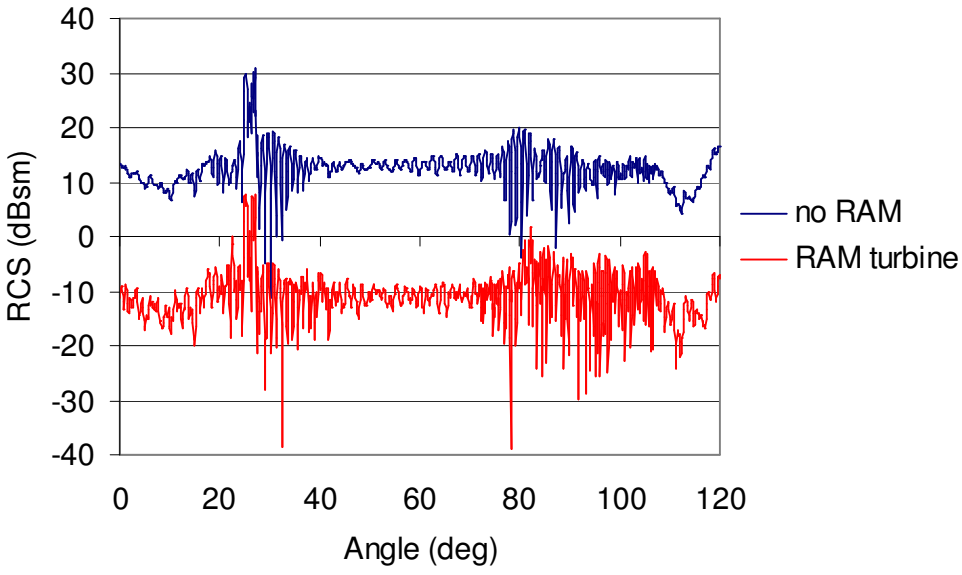

Figure 2-12 RCS for whole turbine RAM (90° yaw)

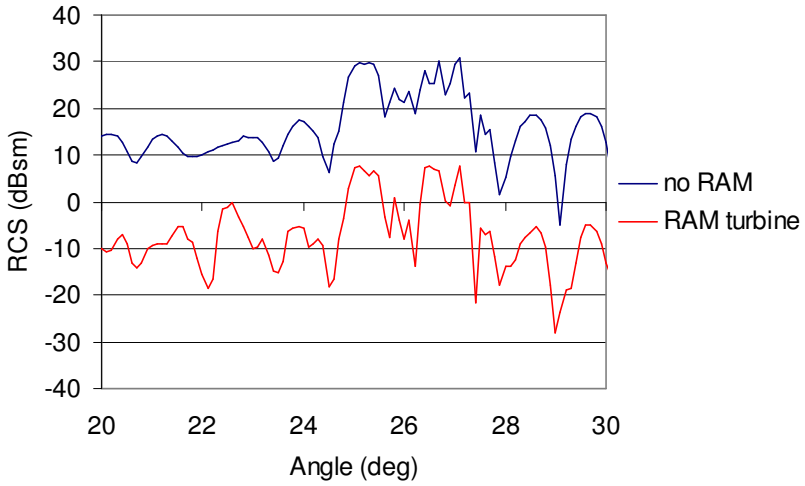

Figure 2-13 Leading edge flash RCS for whole turbine RAM (90° yaw)

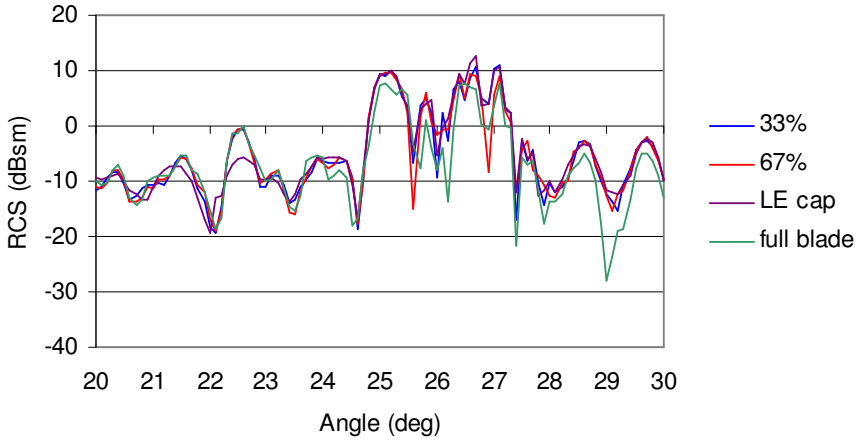

Figure 2-14 Comparison of blade treatments (90° yaw, RAM tower and nacelle)

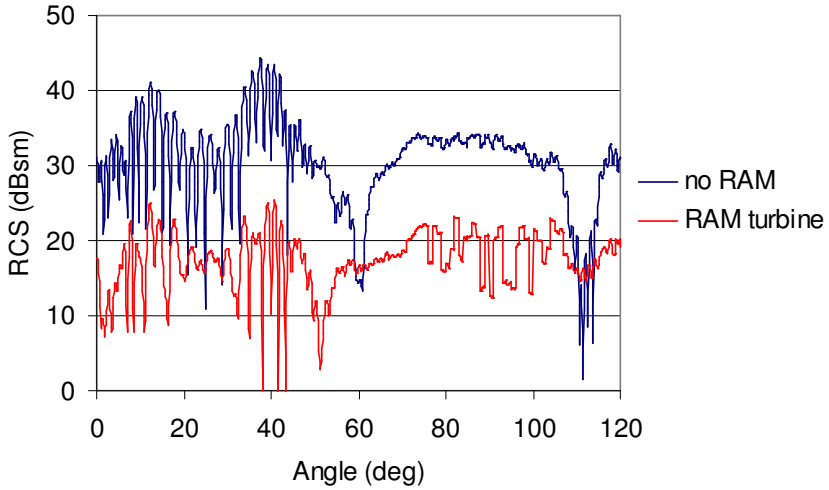

Figure 2-15 RCS of whole turbine RAM (0° yaw)

2.5 Weather and marine navigation radar

2.5.1 Results

2.5.1.1 A similar pattern of results to the ATC case was observed for the weather and marine radar cases – RAM application leads to a reduction in the median and peak RCS at 90° yaw, but smaller reductions for the 0° yaw case. The overall results are summarised in Tables 2-2 and 2-3. The median RCS is of most interest for weather radars, as operators make use of time-averaged data rather than instantaneous features such as blade flashes. The apparent size of the turbine would be significantly reduced even though this is unlikely to prevent detection, due to the sensitivity of the radar. An example RCS prediction is shown in Figure 2-16, for the 90° yaw, marine radar case, as a function of RAM treatment. This clearly shows that full turbine RAM treatment would be needed to reduce the median RCS to below 0dBsm.

		Median RCS		Peak RCS	
		m^2	dBsm	m^2	dBsm
0° yaw	No RAM	100	20.0	676	28.3
	Whole turbine RAM	15	11.9	309	24.9
90° yaw	No RAM	158	22.0	2,188	33.4
	Whole turbine RAM	<0.5	-3.5	20	13.1

Table 2-2 RCS reductions at weather radar frequencies

		Median RCS		Peak RCS	
		m^2	dBsm	m^2	dBsm
0° yaw	No RAM	39	15.9	2,188	33.4
	Whole turbine RAM	7	8.6	200	23.0
90° yaw	No RAM	112	20.5	1,905	32.8
	Whole turbine RAM	<0.5	-4.5	16	12.0

Table 2-3 RCS reductions at marine navigation radar frequencies

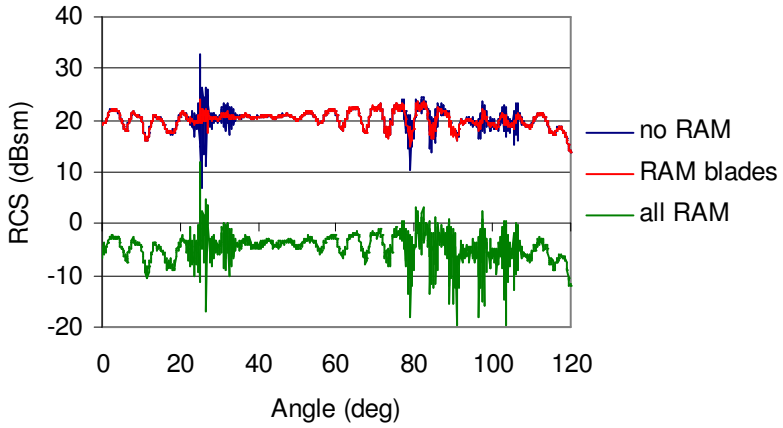

Figure 2-16 RCS for whole turbine RAM (90° yaw, marine radar)

This page is intentionally blank

3

RADAR IMPACT MODELLING

3.1 Nemesis code

3.1.1 The Naval Electromagnetic Environment Simulation Suite, NEMESiS, is a propagation modelling engine designed to model range dependent propagation effects over land and sea for a given azimuthal slice. The model uses an efficient parabolic equation method to solve Maxwell's equations to provide propagation factors over a range vs. height grid (as shown in Figure 3-1). This is then used to provide the user with a variety of different outputs ranging from predicted clutter power returns to probability of detection. By running the model repeatedly, this single slice output can be built up to produce a detection probability output, such as that shown in Figure 3-2 for a fictitious location near the Isle of Wight.

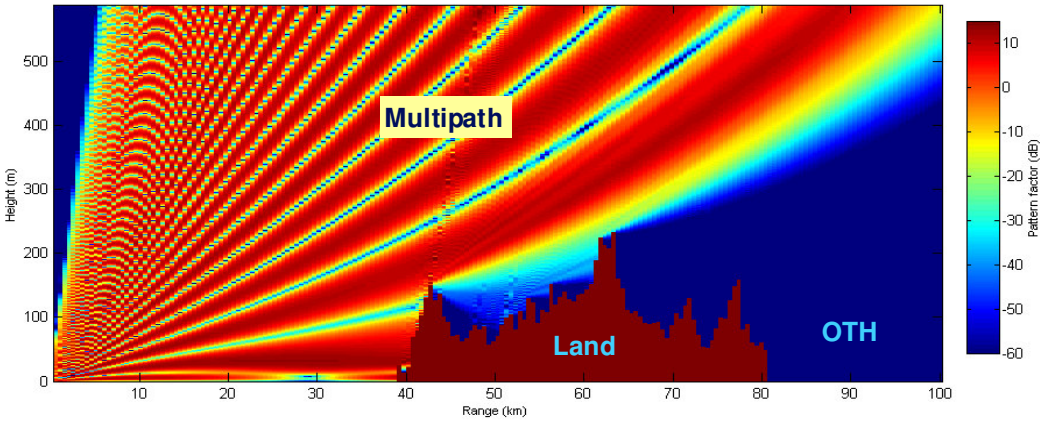

Figure 3-1 NEMESiS propagation factor in a littoral azimuthal slice

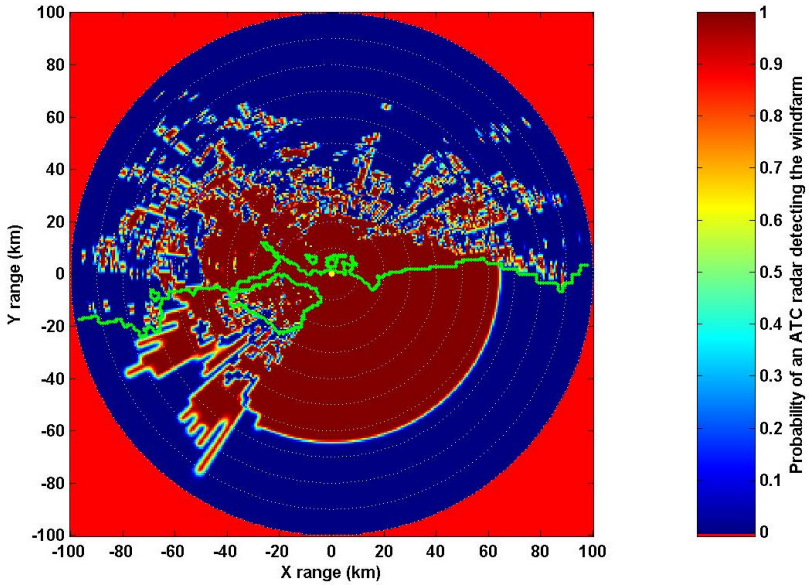

Figure 3-2 NEMESiS output - probability of detection

3.1.2 For this study, the visibility of a wind farm site to a particular type of radar system has been assessed. To run the radar model for every range and azimuth for hundreds of miles around a wind farm site would be impossible, so the principle of reciprocity, implicit from Maxwell's equations, has been used. The 'radar' is sited on the wind farm at the wind farm height and the visibility of any radar site is assessed by calculating 'target' returns for a target with the RCS of the wind farm, at the height of the radar. If the 'target' is detected then the wind farm would be detectable to the radar. This builds up a detailed visibility map of the type shown in the left-hand plot of Figure 3-2.

3.2 Radar parameters

3.2.1 Table 3-1 lists the radar parameters obtained for the NEMESiS propagation simulations of the three generic radar types considered in this study. It refers out to Table 3-2, which explains the source of these values.

3.2.2 It is seen in Table 3-1 that not all the obtained radar parameters could be modelled using the NEMESiS software without prohibitively time-consuming modifications to the code. Consequently, these parameters have been replaced in the simulations with the nearest suitable alternative, as described in the notes accompanying Table 3-1. Specifically, these alterations affect the description of some radar beam patterns and polarisation. When considering the extent of range coverage of the radar for a specific target description these parameters are not critical and should have negligible affect on the results. In such a scenario, the radar height, gain and peak power are much more important factors.

3.2.3 The parameters described in Table 3-1 are typical descriptions of radar serving those purposes ascribed to them. Radar design is renowned for being tailored to the specific purpose intended in any given use. This means that, for example, many ATC radar systems will operate at a different frequency to that described in Table 3-1. However, the values quoted are intended to be typical. Between the three radar types considered and listed in Table 3-1, a range of frequencies, peak power and pulse lengths have been covered.

Radar parameter	ATC Radar	Weather Radar	Maritime Radar
Frequency (GHz)	2.885 [A]	5.625 [C]	9.1375 [D]
Typical height (m)	35m AMSL [A]	15m + terrain [C]	57m + terrain [E]
Peak power (kW)	12 [A]	250 [C]	25 [F]
Pulse duration (μs)	0.8 [A]	2.0 [C]	0.25 [E]
Polarisation	Circular [A] [c]	Vertical [C]	Circular [D] [c]
Transmit gain (dB)	33.4 [A]	43 [C]	38 [F]
Receive gain (dB)	33.4 [A]	43 [C]	38 [F]
Loss (dB)	1.5 [A]	2 [C]	5 [G]

Noise (dB)	2.5 [B]	9 [C] [b]	3.5 [F]
Noise (W/Hz)	$7.117*10^{-21}$ [B] [a]	$3.162*10^{-20}$ [C] [b]	$8.959*10^{-21}$ [F] [a]
CFAR[d] level	10^{-6} [B]	n/applicable [C] [f]	10^{-4} [G]
Beam pattern	Cscsq [A]	Gaussian [C] [e]	Fan [F] [f]
Elevation (°)	2 [A]	0 [C]	0 [G]
Elevation beamwidth (°)	40 [A]	1 [C]	12 [E]
Azimuthal beamwidth (°)	1.5 [A]	1 [C]	0.4 [E]

Table 3-1 Radar Parameters used in NEMESiS predictions

(a) Calculated from the decibels quoted value, to obtain the correct units for NEMESiS.
(b) Calculated indirectly from other data supplied.
(c) Horizontal polarisation substituted for circular in NEMESiS simulations. This makes little difference to the propagation result.
(d) CFAR – Constant False Alarm Rate
(e) High nominal value of 0.1 used in NEMESiS calculations.
(f) 'Sinc' beam pattern substituted for quoted one in NEMESiS simulations. This makes little difference to the propagation result of the main beam.

Reference in Table 1	Source
[A]	Parameter used to replicate the Prestwick airport ATC radar, provided by the authors of [1].
[B]	Generic ATC radar parameter taken from [4].
[C]	Parameter provided by email from the UK Meteorological Office. Thanks to Mike Edwards for correspondence.
[D]	Parameter used to replicate the Holland Haven PLA radar on the Thames estuary, taken from [3].
[E]	Parameter used to replicate the Holland Haven PLA radar on the Thames estuary, taken from [5].
[F]	Parameter used to replicate the Holland Haven PLA radar on the Thames estuary, taken from the Terma "Scanter 2001 Vessel Traffic Monitoring and Coastal Surveillance Application" radar brochure available via www.terma.com (07/01/2004).
[G]	Estimated value from experience within QinetiQ.

Table 3-2 Explanation of the sources of information given in Table 2

3.3 Cases modelled

3.3.1 Figures 3-3 and 3-4 show the terrain surrounding the two chosen sites for the radar propagation analysis. Figure 3-3 shows an imaginary wind farm site in the Wash, whilst Figure 3-4 shows the terrain around the Hare Hill site. Both show the digital terrain data out to a range of 150km, enough to include the extremities of propagation for the radar types considered here.

3.3.2 The Wash has been earmarked as a designated area for offshore wind farm development by the UK government. It also provides a relatively simple propagation environment due to the flat nature of the surrounding terrain, with one sector in azimuth open to the North Sea. The exact site chosen is at latitude 53:00:19 North, longitude 00:17:37 East, roughly four miles off the Lincolnshire coast between Boston and Skegness. Although the coastline is clearly recognisable in Figure 3-3, some inland terrain in Lincolnshire and Cambridgeshire actually appears blue as it is beneath sea level. This was chosen as a suitable site for predictions of detection by weather and marine radar systems.

3.3.3 The site at Hare Hill in Scotland already has an operational wind farm consisting of 20 turbines. It has been chosen in this study as a site that has experienced radar interference with Prestwick airport ATC radar and also had previous investigations focused on it [1]. It is located at latitude 55:21:06 North, longitude 04:07:04 West, to the South West of Glasgow and Kilmarnock. The site is more complicated than that in the Wash from a propagation point of view. The area generally has a much higher elevation and is rugged terrain, which will in turn lead to more diffraction and other interference of the radar signal.

3.3.4 For each turbine blade design considered by this work, two values of turbine RCS were generated. Intuitively, the height of a target above the local terrain level will affect its visibility to radar, and this is reflected in the NEMESiS modelling performed here. It is therefore necessary to choose a suitable height for any given RCS value.

3.3.5 The first value represented a median RCS that would typically be present for most turbine blade positions during rotation. This value was modelled as if present at a height equal to the centre of the turbine nacelle. This was chosen as the centre of the highest static component of the turbine and so likely to contribute significantly to this background level of RCS.

3.3.6 The second value was a peak value obtained during rotation of the blades, normally due to the instantaneous vertical positioning of a blade during rotation. This geometry would momentarily present the radar with a perpendicular length of blade from which an increased level of reflection would occur. This value was taken to be at a height given by the sum of the nacelle height plus the blade length; the highest level any part of the turbine reaches. In this respect these simulations can be considered as ‘worst case’:

the turbine has its peak reflectivity modelled at its highest point during rotation.

3.3.7 The range of cases reported here is described in Table 3-2. The ATC and marine navigation results include median and peak RCS cases, but only median RCS results are shown for weather radar, since time-averaged detection is more relevant in that case.

	Hare Hill		The Wash	
	Median RCS	Peak RCS	Median RCS	Peak RCS
ATC	✓	✓		
Weather			✓	
Marine			✓	✓

Table 3-2 Summary of detection probability cases reported

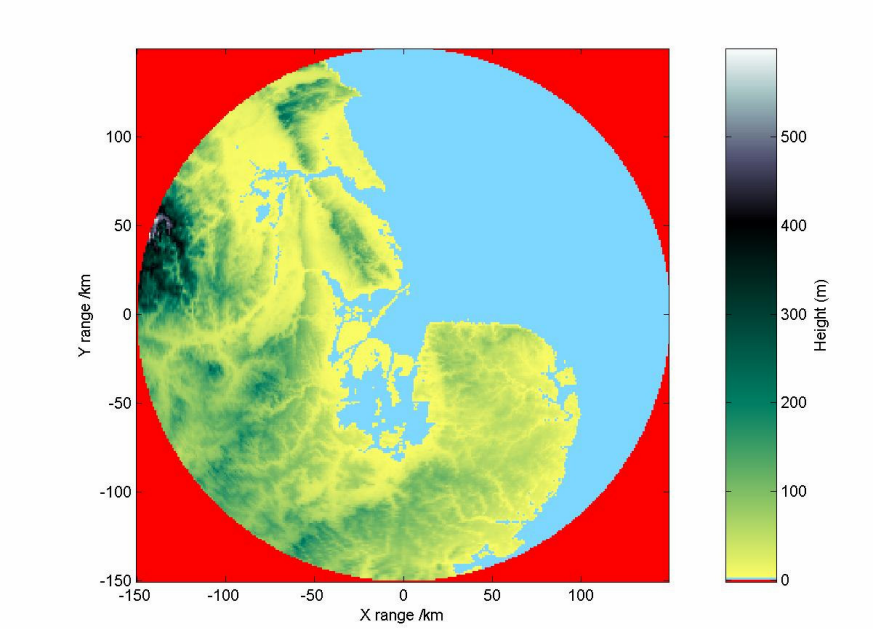

Figure 3-3 Digital terrain data around the chosen offshore site in the Wash.

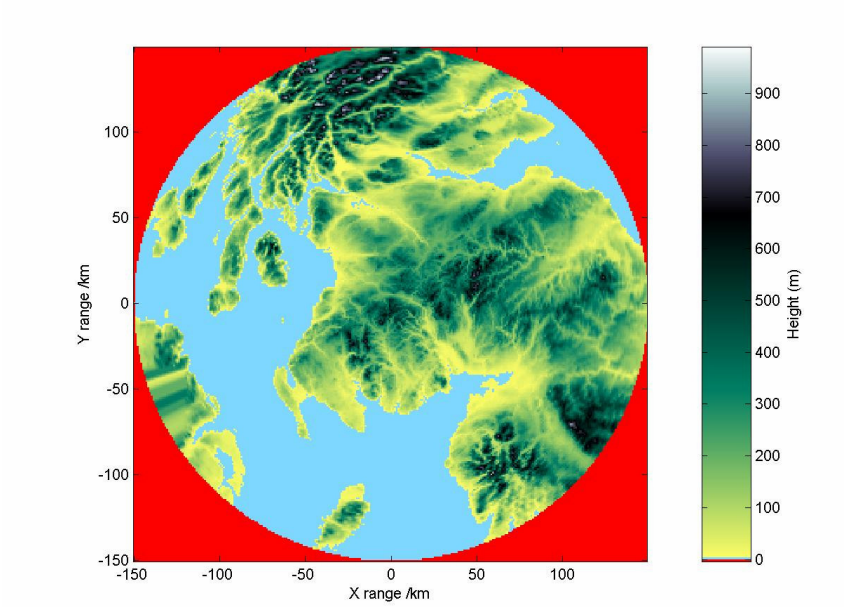

Figure 3-4 Digital terrain data around the Hare Hill wind farm site.

3.4 Results

3.4.1 Introduction

3.4.1.1 The Figures in this section show the area within which the radar type concerned would be able to detect the turbine being modelled if it was located at the centre of the chart, and with what probability. Typically, the probability drops from 1 (certain to detect the turbine) to 0 (will not detect the turbine) over a short distance at the edge of the detection area. This is demonstrated by the rapid shift in colour at the edge of the detection area, representing rapidly changing probability on the colour scale. Local coastal outlines have been added to the chart to aid visual recognition of the area.

3.4.2 ATC Results

3.4.2.1 Most of the reported problems with wind farm interference on radar displays have arisen from users of ATC radar, both civil and military. This report does not consider military systems, but results for the previously described civilian ATC radar are presented here. As shown in Table 3-2, the ATC cases are restricted to the Hare Hill site, for the original (non-RAM) turbine and the full RAM turbine, and for median RCS and peak RCS values.

3.4.2.2 Figure 3-5 shows the probability of detection of the non-RAM turbine and full-RAM turbine, for median RCS. The position of Prestwick airport has been marked with a white circle, for reference, and the dotted radial lines are spaced at 10km intervals. It is evident that the non-RAM turbine would be detected by the ATC radar located at the airport. In this median RCS case, in which the RCS has been reduced to -10dBsm, the range at which

the turbine is detected is greatly reduced. As this is the most frequent configuration in which the turbine would be viewed, this is a significant result and indicates that the number of false radar plots ought to be drastically reduced.

3.4.2.3 The peak RCS case shown in Figure 3-6 results in a higher probability of detection than the median case, but the use of RAM does reduce the detection probability compared to the non-RAM turbine case. The effect of a Doppler filter is not included in these results, and it is expected that the detection probability would decrease further in reality. The maximum range at which a high probability of detection is recorded is larger for the peak RCS case, in comparison to the median case. The detection area is still fragmented, but now has areas of high probability of detection at large ranges in excess of 100km. This is due to diffraction of the radiation over rugged terrain along its propagation path, which can serve to enhance the energy falling on certain areas if the geometry is right.

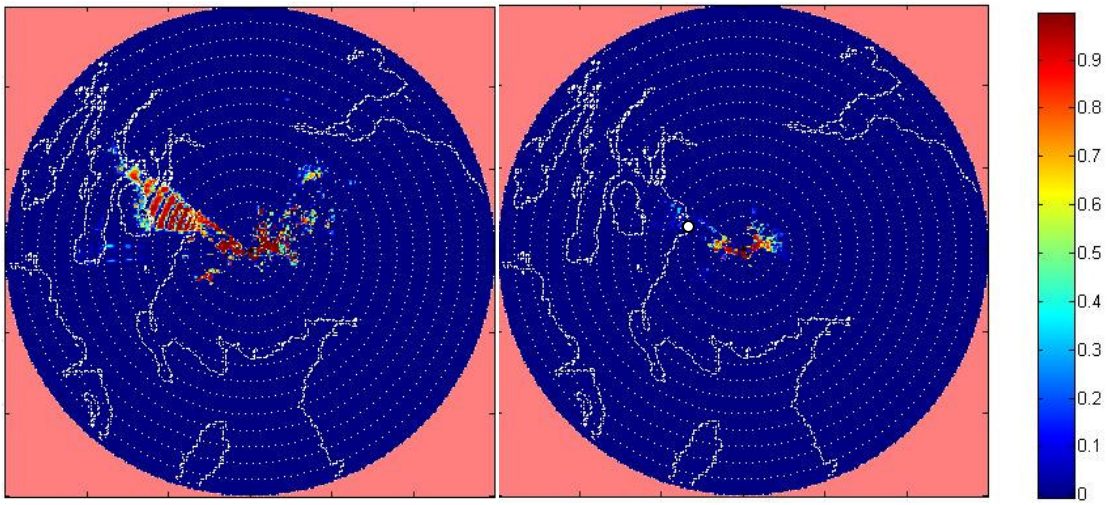

Figure 3-5 Probability of detection - ATC radar, Hare Hill, median RCS (90° yaw) non-RAM (left) and full RAM (right)

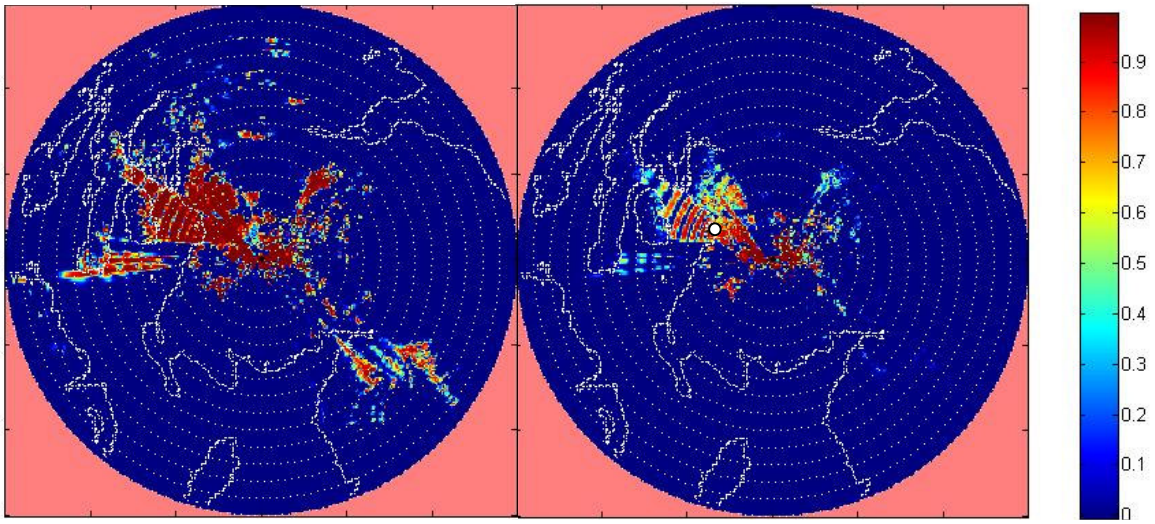

Figure 3-6 Probability of detection - ATC radar, Hare Hill, peak RCS (90° yaw) non- RAM (left) and full RAM (right)

3.4.2.4 The rugged terrain surrounding the site results in a highly fractured area in which ATC radar of the type chosen would be able to detect the turbine. In general, the terrain has minimised the range at which the turbine is visible to such radar. However, one sector in azimuth, to the Northwest, maintains a high probability of detection of the turbine out to a range of approximately 70km. This is due to the local terrain immediately around the Hare Hill site.

3.4.2.5 The site is on a north-facing hillside of a valley running east-west in direction. To the east, this valley turns southwards, and beyond this to the east lies more high terrain. On the other hand, the western end of the valley shallows out towards the sea, enabling radar in this area a relatively clear view of the turbine. Once over the sea, the view is obviously unbroken, leading to the elevated probability of detection out to large ranges. To the east of the site, only intermittent, broken areas of visibility remain due to the specifics of the rugged terrain.

3.4.3 Weather radar

3.4.3.1 Weather radars are somewhat different in nature to the other types considered in this study. They gather information over slower periods of time than either ATC or maritime navigation radar and are not directly safety critical (although the information they provide along with other sources is used for safety reasons by a variety of users). They do not search for targets as such, a point reflected by their lack of a CFAR in Table 3-1.

3.4.3.2 For this reason, any single observation by a weather radar is less important than the general trend observed. This study reflects this by considering only the median RCS value of the turbine. Any peaks due to ideal blade

orientation are assumed to be sufficiently transient compared to operational timescales as to be unimportant.

3.4.3.3 The effect of the increased power of the meteorological radar is to push the horizon limited maximum detection range over the seaward azimuth further out in range than would be the case for the ATC radar described previously.

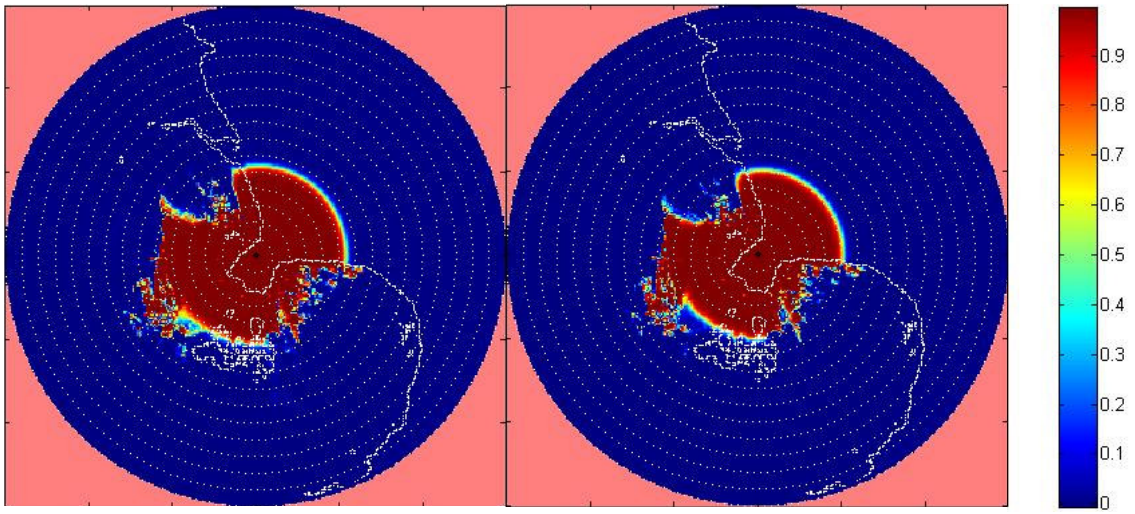

Figure 3-7 Probability of detection - Weather radar, The Wash, median RCS (0° yaw)
non-RAM (left) and full RAM (right)

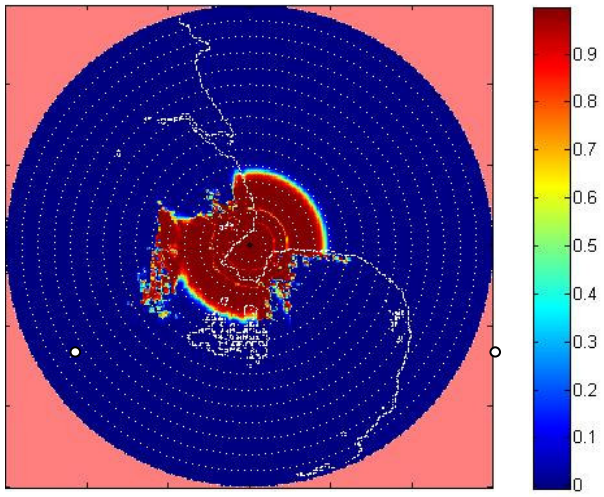

Figure 3-8 Probability of detection - Weather radar, The Wash, median RCS (90° yaw) full RAM

3.4.3.4 The weather radar results are shown in Figures 3-7 and 3-8, for the median RCS case only. These provide an example of horizon limited detection in the azimuth sector pointing towards the North Sea. As there is no terrain modifying the propagation in this direction, the radiation travels as far as the horizon will allow, resulting in the smooth, arc shaped cut off of

probability of detection over the sea. The reduction in median RCS from 20.0 dBsm to 11.9dBsm (0° yaw) reduces the maximum detection range by ~3km. The reduction from 22.0dBsm to -3.5dBsm (90° yaw) has slightly more impact, but the turbine is still detected at ranges up to 22km. As the Wash area of the UK mainland is relatively flat terrain, these Figures show little deviation from this behaviour in other azimuth directions.

3.4.4 Marine navigation radar

3.4.4.1 The impact of the RAM turbine on detection by marine navigation radar is shown in Figure 3-9 for the 0° yaw case and Figure 3-10 for the 90° yaw case, both calculated from median RCS. The RCS values used were 8.6dBsm (7.2m^2) and -4.5dBsm (<0.5m^2), respectively. There is an apparent reduction in the detectability of the turbine at 0° yaw, though detection can still occur at 25km range, compared to just under 30km for the non-RAM turbine. However, the 100% detection range decreases to less than 10km for the much lower RCS at 90° yaw, a reduction of nearly 20km.

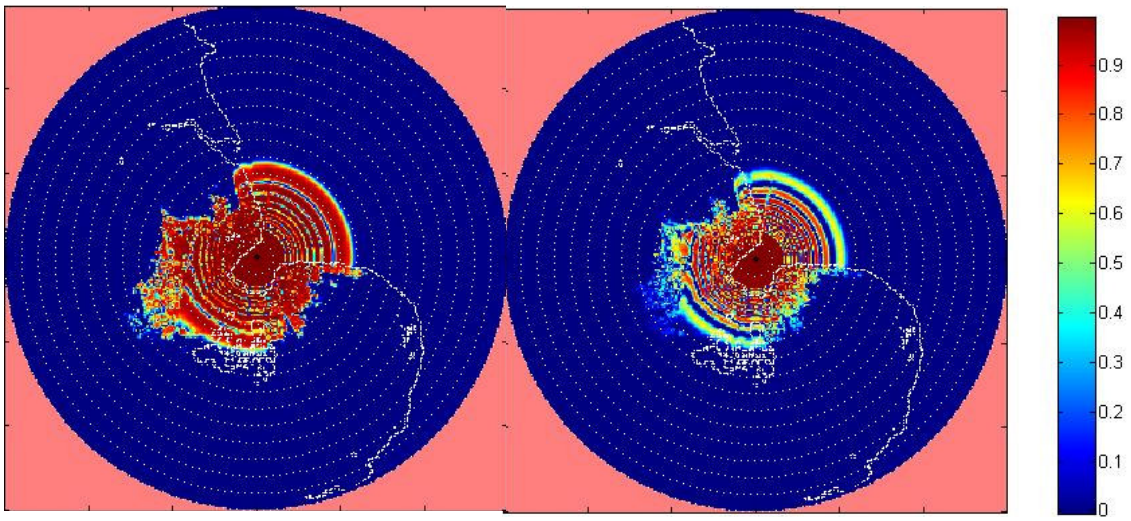

Figure 3-9 Probability of detection - marine radar, The Wash, median RCS (0° yaw) non-RAM (left) and full RAM (right)

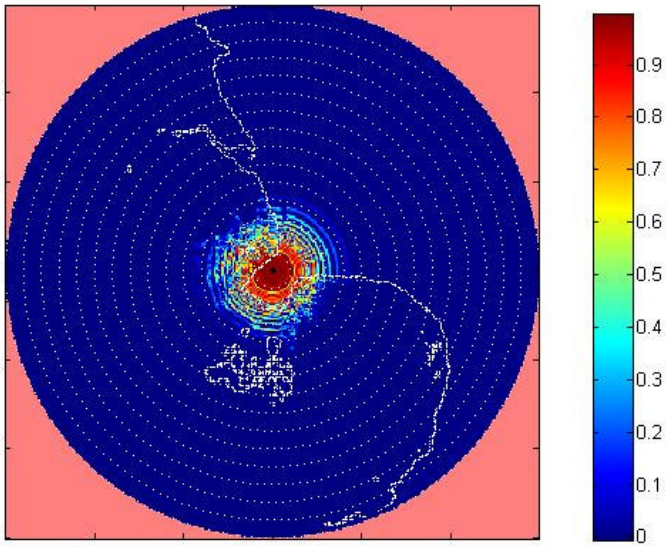

Figure 3-10 Probability of detection - marine radar, The Wash, median RCS (90° yaw)
full RAM (right)

This page is intentionally blank

4 DESIGN AND MANUFACTURE OF BLADE RAM

4.1 Materials characterisation

4.1.1 The first step towards re-designing the composite blade to create a radar absorbent version is to understand the electromagnetic properties of all constituent materials. The construction is shown schematically in Figure 4-1 for a position away from the root section. The thicknesses of the various foam and glass fibre reinforced epoxy (GRE) layers vary with position along the blade length, and the root section (where the blade attaches to the turbine hub) is a solid GRE composite.

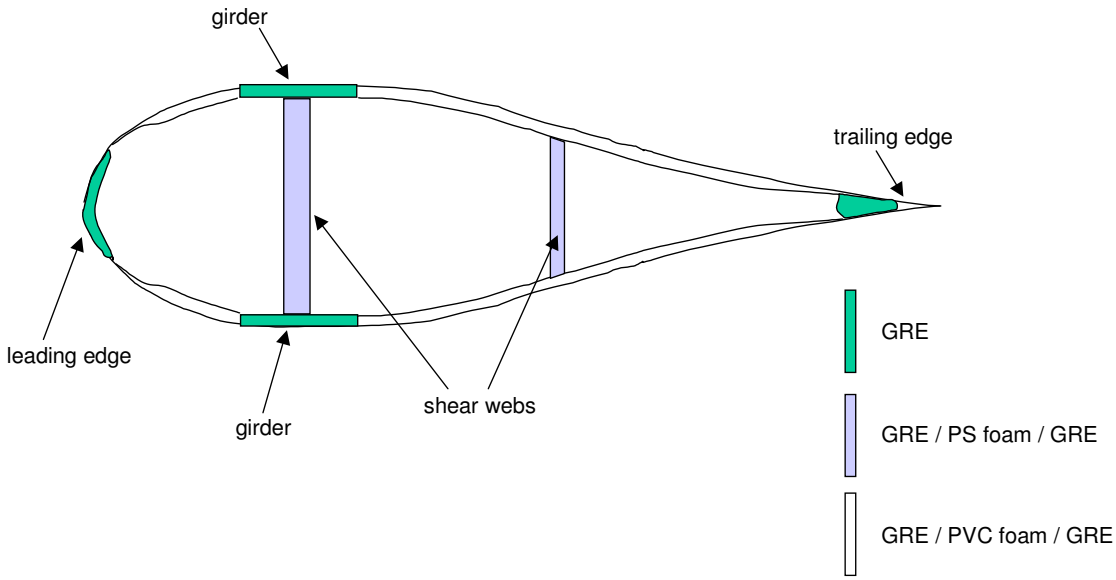

Figure 4-1 Schematic of the typical construction used in NOI 34m blade

4.1.2 The majority of the surface area of the blade comprises GRE/foam sandwich material. The solid GRE girders and the GRE/foam sandwich shear webs (which together give the blade its structural strength and prevent twist) are made separately and then integrated into the blade during assembly. The girders are included in the lay-up of the upper and lower halves of the blades, whereas the shear webs are bonded into place when the two halves are brought together. The leading edge region is sealed using a pre-produced GRE insert and resin, whereas the trailing edge region is sealed with a foam insert and resin.

4.1.3 A wide selection of samples was supplied to QinetiQ by NOI for evaluation of electromagnetic properties. The most important of these were:

- GRE/foam/GRE sandwich panel PVC foam, 10-20mm, main surface
- unidirectional GRE girders
- shear web foam polystyrene (PS) foam, thickness 20-40mm

GRE skins were separated from the sandwich panel foam for measurement.

4.1.4 The dielectric constant of samples was calculated from measurements of their complex reflection coefficient (i.e. magnitude and phase) made in the microwave frequency region 1 to 12 GHz, using a vector network analyser. Some measurements were made in waveguide cells, on samples machined to size. Some were made using a coaxial probe on samples with flat surfaces and larger foam samples were measured in a free-space reflectometer system. Results were converted into a form suitable for input to QinetiQ's absorber design codes.

4.1.5 Measured results are as one would expect from standard foams and GRE. The foam has a low dielectric constant, , with very little loss, whereas the GRE varies between =3.25 and =3.5, depending on whether the sample under test is taken from the outer or inner skin (both show a loss tangent of <0.1).

4.2 Blade reflectivity study

4.2.1 Previous predictions [1] of the RCS of wind turbines had shown some discrepancies in the magnitude of RCS even though the time-dependency was well predicted. The authors attributed these to incorrect assumptions about the blade material reflectivity. It was felt that a study of the construction details of the blade would help not only in the RAM design activity, but would also clarify the exact nature of the scatter of radar by the blade.

4.2.1 A section of blade was supplied by NOI so that QinetiQ could evaluate the leading edge (LE) and trailing edge (TE) regions and the general construction. During this evaluation, the reflection of signals in the 2-10 GHz range from the LE and TE was measured using a pair of antennas connected to a vector network analyser. As well as providing a measure of the reflectivity as a function of frequency, the analyser can transform from the frequency domain to the time domain, effectively creating a 'time of flight' measurement for an equivalent pulse. In this mode it is possible to resolve reflections that come from the LE (or TE) and the internal parts of the blade, such as the edges of the girders and the primary and secondary shear webs, due to their different distances of travel. This is a standard technique often used to identify faults in microwave cables and devices.

4.2.2 Figure 4-2 shows the time domain response from the LE illuminated at normal incidence, with the electric field parallel to the length of the edge (the result for the perpendicular polarisation condition was almost identical). The peak at 0ns represents the reflection from the front of the LE, and reflections from within the blade are at positive times. Two traces are shown: one from the whole depth of the blade and the other taken with a reflective metal coating applied to the rear of the primary shear web. The

increased amplitude of the signal returning from the rear of the web (located at 4.6ns) with the metal applied demonstrates that appreciable levels of signal penetrate through the LE and the web. The frequency dependence of reflectivity is shown in Figure 4-3, from which it is evident that reflectivity is high at 3 GHz, but lower between 4 and 7 GHz (for this particular configuration of antennas and blade), demonstrating that some frequencies do penetrate into the blade interior. Data are also shown in Figure 4-3 for 1-D reflectivity predictions made for the LE + primary shear web only (i.e. assuming that only air exists behind the primary web). The general agreement with the measured reflectivity data is evident, despite being modelled as an infinitely wide planar material, which is clearly not the case for the blade measurement.

4.2.3 It has been shown that the LE region is highly reflective and is a dominant contributor to the peak RCS at ATC radar frequencies. The GRE insert and additional glass cloths laid over the LE region during finishing must be carefully controlled and designed to form a high performance RAM, if peak RCS levels are to be reduced.

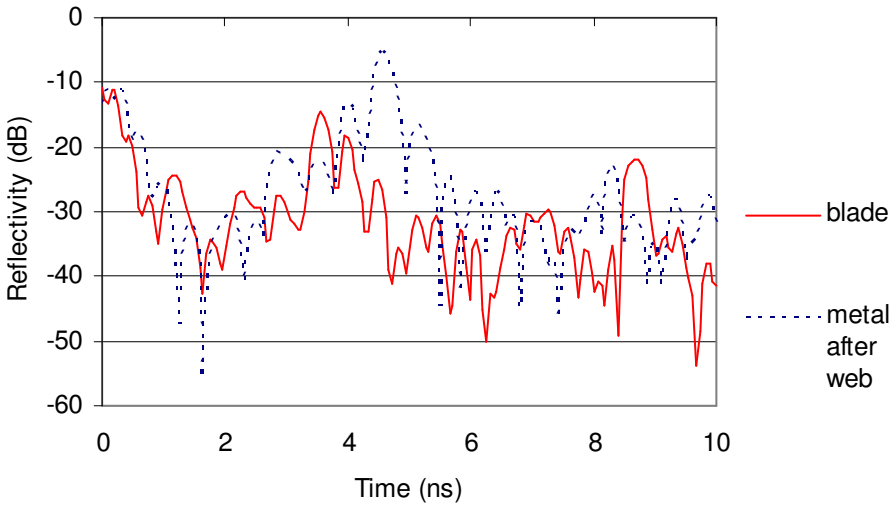

Figure 4-2 Time domain response from leading edge

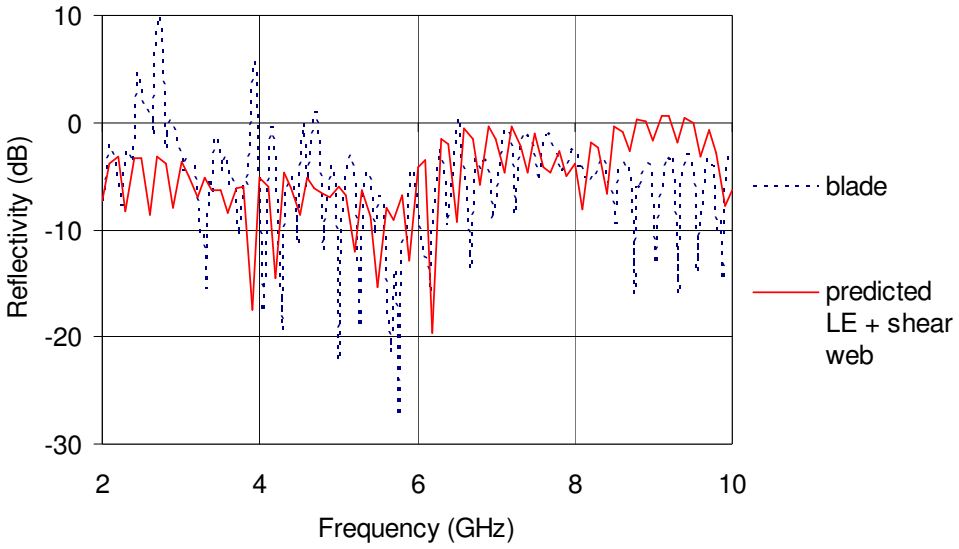

Figure 4-3 Measured and predicted frequency domain response from leading edge

4.2.4 Corresponding results for the TE are shown in Figures 4-4 and 4-5, for time- and frequency-domains, respectively. Although the shaping of the TE results in less energy penetrating the blade, it is still clear that signals pass through the TE and the secondary shear web and are reflected back through the TE. Figure 4-4 shows results for the blade both untreated and with metal applied behind the secondary shear web.

4.2.5 The possibility of diffraction of signals by the resin-filled foam sections was investigated theoretically and by experimental measurement of samples produced by NOI. Predictive code developed by QinetiQ was used to identify any non-specular reflections in the frequency range 1-10 GHz, over 0-90° angles of incidence and in both vertical and horizontal polarisations. The results for a metal-backed GRE/6mm foam/GRE sandwich are shown in Figure 4-6. This shows that the maximum total diffracted signal is only ~1% of the incident signal, and that it is confined mostly to high angles of incidence and frequencies above 5 GHz, having no impact on absorbing blades intended to counter ATC radar problems.

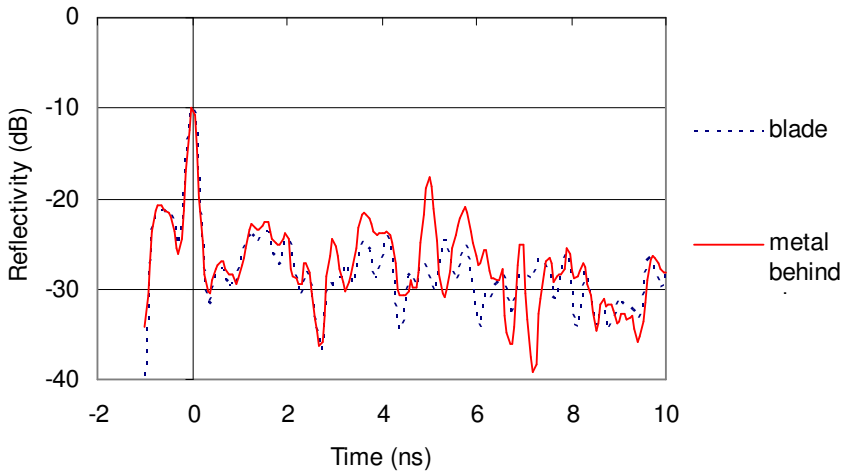

Figure 4-4 Time domain response from trailing edge

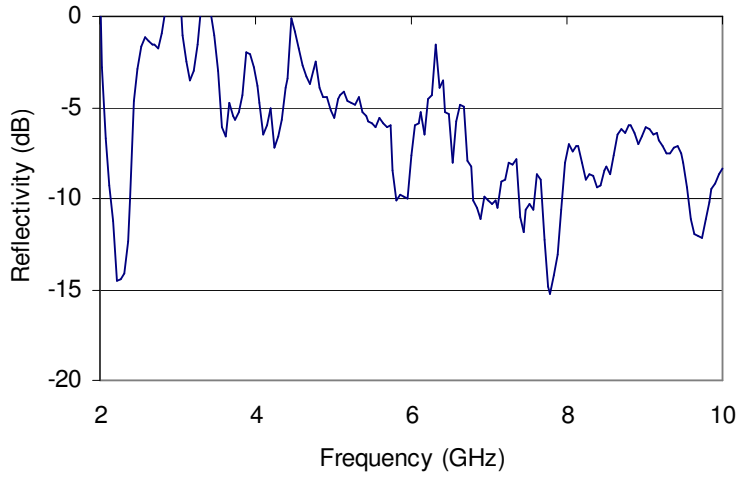

Figure 4-5 Frequency domain response from trailing edge

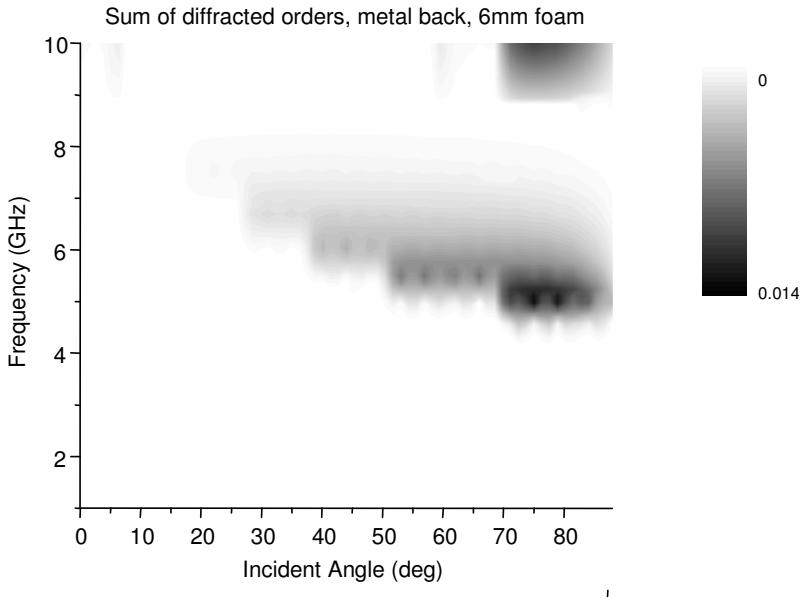

Figure 4-6 Diffraction from metal-backed GRE/6mm foam sandwich panel

4.3 Design of RAM

4.3.1 RAM descriptions

4.3.1.1 The different materials that are found around the blade surface offer opportunities for the RAM designer to modify these to create absorbers of two types; either Dallenbach RAM or Jaumann RAM, and so a description of each is merited.

4.3.1.2 The *Dallenbach absorber* comprises an inherently absorbing material; for example, a host matrix doped with absorbing filler particles and backed by a perfect electrical conductor (PEC). If the electrical thickness of a material (which is equal to the physical thickness multiplied by $(\ )^{1/2}$, where and are the material dielectric and magnetic constants) is made equal to a quarter wavelength at the frequency of interest, then a resonant absorption occurs. The absorption has a finite frequency bandwidth. This can be increased (though this is often not necessary) by creating several layers, with increasing filler concentration from the layer nearest to the PEC outwards, giving a better impedance match to the incoming radar signal. Harmonics are generated that combine to give better broadband performance.

4.3.1.3 A Dallenbach absorber could be created in the GRP/foam/GRP blade construction by replacing the foam with an absorbing variant. Having studied the typical section dimensions of the NOI blades, it is clear that there is sufficient thickness (and hence electrical thickness) to create a RAM that operates at the frequencies of interest. The PEC would be created by insertion of a carbon-fibre cloth layer into the rear GRP skin.

4.3.1.4 In principle, it is possible to modify most regions of the blade to form Dallenbach RAM. However, the unidirectional GRE girders and GRE root sections do not lend themselves to this approach on structural grounds (i.e. inclusion of large quantities of filler particles would significantly alter the physical strength of the GRP) and commercial RAM foams tend to be expensive.

4.3.1.5 The *Jaumann* absorber is a more suitable choice, since it is simpler to realise in blade materials. In its basic form, it is created by placing a resistive layer at a specific spacing from a PEC, as shown in Figure 4-7. The graph in Figure 4-8 shows the reflectance of a Jaumann RAM comprising a 377 ohms/sq. resistive layer, in a epoxy/glass fibre GRP panel (-dB represents absorption). In practice one might not use a simple resistive layer, but would instead use a lossy impedance layer that can give better control over absorption. Impedance layers can be made (for example) from glass fibre tissues impregnated with a small amount (typically a few wt%) of chopped carbon fibres, and are available commercially. Such an approach is attractive in this project because it involves modifications to glass cloth layers that are used as standard in blade manufacture.

4.3.1.6 The narrow bandwidth of the Jaumann RAM can be increased, in a manner analogous to that used for the Dallenbach absorber, by using two or more lossy layers spaced appropriate distances from the PEC to give absorption at the required frequencies. The reflectance of 2- and 3-layer versions is also shown in Figure 4-8. It is clear that wider frequency bandwidth can be achieved by the addition of extra layers, if this is required.

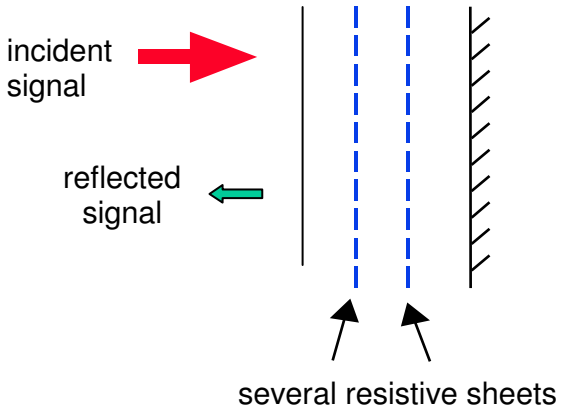

Figure 4-7 The Jaumann absorber

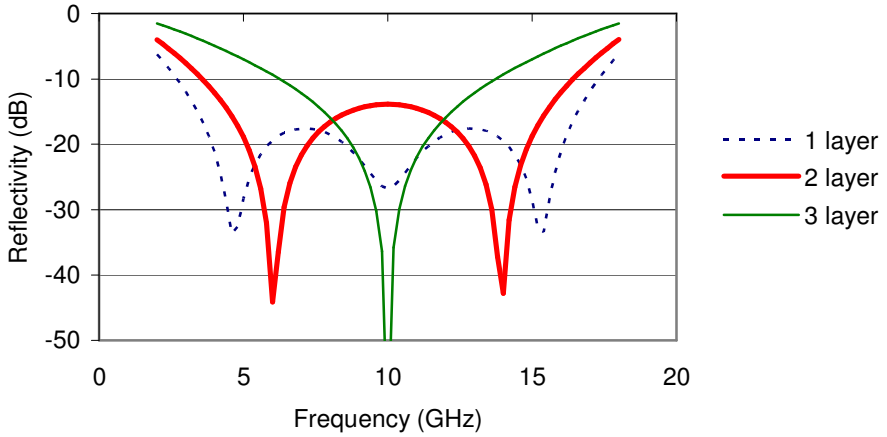

Figure 4-8 Performance of Salisbury screen and Jaumann RAMs

4.3.2 Sandwich panel RAM

4.3.2.1 Much of the surface area of the 34m NOI blade comprises a sandwich panel constructed from GRE and PVC foam. It is feasible to replace the standard foam with a modified version that is loaded with absorbing filler particles, to form a Dallenbach RAM. However, the preferred option from the viewpoint of maintaining structural integrity is to use standard foam and to create a Jaumann RAM by modifying the outermost GRE skin using a lossy impedance layer based on glass cloth. The mechanical strength of the sandwich panel suffers no degradation because the modification is made within the GRP skin and hence cannot affect the bond between skin and foam. The thickness of the sandwich panel varies along the length of the blade, varying from 20mm near the blade root to 10mm near the tip. A very small section at the root is 6mm thick, but there is thick GRE beneath and this foam thickness was not taken as a special case. Obviously it will not be possible to create a single RAM for the whole blade, but many parts may be modified in this way to create RAM sandwich panels.

4.3.2.2 It is interesting to predict the performance of a Jaumann RAM for a simple resistive sheet (377 ohms/sq.) placed on the outer surface of foam thickness 10 and 20mm. Figure 4-9 shows such predictions, which assume a reflector on the inside surface of the sandwich. In the 20mm case, absorption can be obtained very close to the 3 GHz (ATC) target frequency and there is a fortuitous harmonic near to the 9 GHz (marine navigation) target. However, the 10mm version has its first absorption maximum near the 5.6 GHz (weather) target and it is not possible to modify the structure to move the absorption to 3 GHz. Clearly a different approach is required for cases where the foam thickness is too small to create absorption at long wavelengths. The approach taken here has been to modify the glass cloths such that they have appropriate complex impedance, rather than purely resistive, properties. Such an approach is feasible, however the difficulty lies in achieving the required impedance components, namely the

resistance (real) and reactance (imaginary). QinetiQ's previous stealth materials expertise was brought to bear on such cases.

4.3.2.3 Variations in pitch of the blades and in azimuth of the turbine mean that absorption may be required over a range of incidence angles and polarisations. The performance of a 22mm thick GRE/PVC foam sandwich tuned for use at 3 GHz degrades with increasing angle, as shown in Figure 4-10, but maintains >20dB absorption to 25° (parallel polarisation) and 30° (perpendicular polarisation). This may be adequate, because the blade flash also decreases as the pitch angle increases from 0°, which is the worst Doppler case.

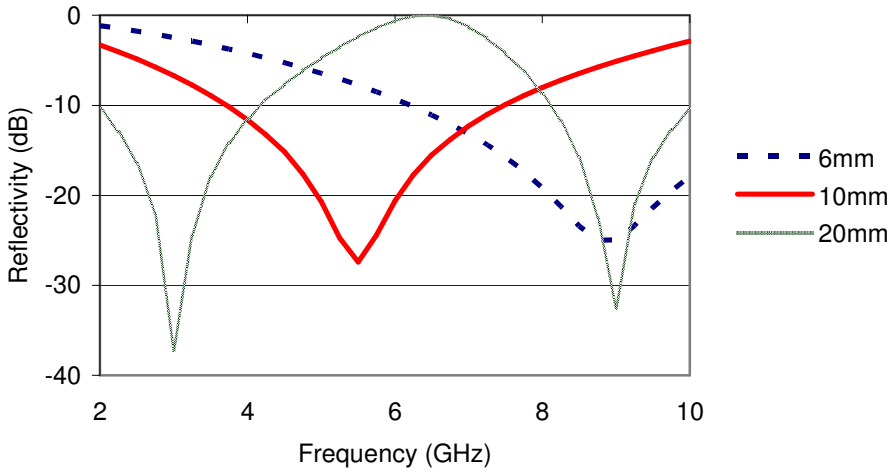

Figure 4-9 Predicted reflectivity of GRE/PVC foam sandwich structures (normal incidence)

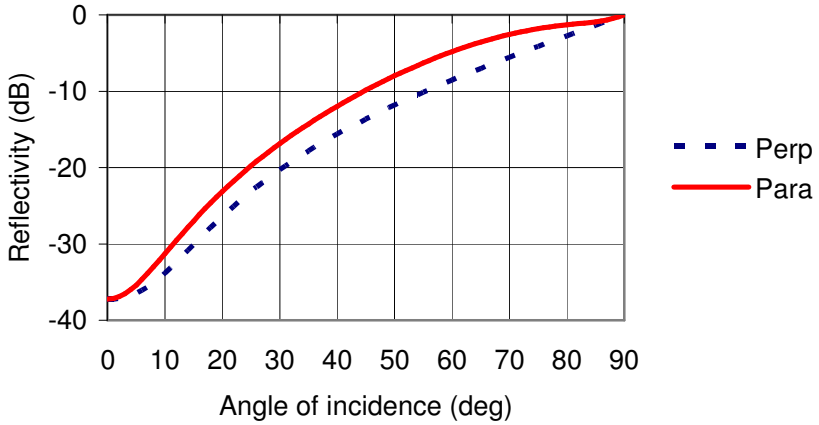

Figure 4-10 Angle-dependence of reflectivity for 22mm thick GRE/PVC foam sandwich structure (3 GHz)

4.3.3 GRE RAM

4.3.3.1 The solid GRE regions that may require treatment to form RAM are the root section, girder and the LE insert. The thicknesses of these regions are adequate for the introduction of RAM for any of the frequencies in question. A Jaumann RAM can be formed by including a lossy layer near the outer surface of the GRE, and a thin carbon cloth layer on the inside surface or within the GRE to act as a conductor. Neither layer will have a significant detrimental effect on structural integrity, as the cloths are designed for use in composite materials.

4.3.3.2 Figure 4-11 uses the predicted performance of 13mm and 20mm GRE Jaumann RAMs, as an example of what can be achieved. The 13mm thick RAM is tuned for ATC frequencies and has a coincidental absorption peak near the 9.14 GHz marine navigation frequency. Similarly, the 20mm thick RAM results in high absorption near weather radar and marine navigation frequencies. By suitable modification of the impedance properties of the lossy layers, these absorption peaks can be tuned to occur at the required problem frequency. It may also be possible to absorb at more than one frequency, should the need arise.

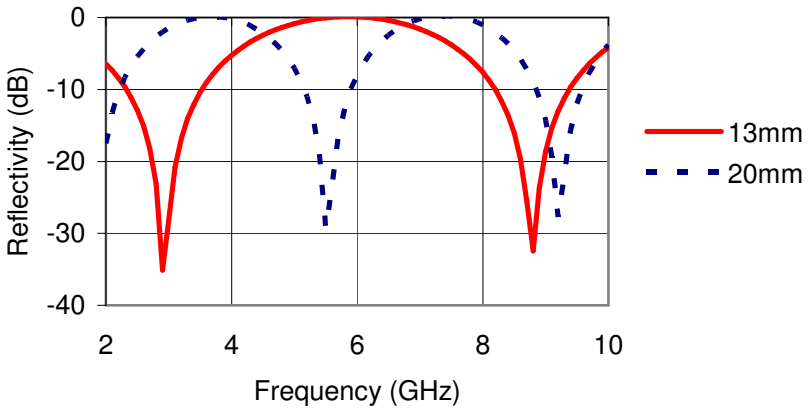

Figure 4-11 Performance of solid GRE RAMs

4.4 RAM manufacture and test

4.4.1 Manufacturing method

4.4.1.1 The NOI blades are made from the component materials described in Section 4.1.3, using the RIFT process – Resin Infusion under Flexible Tooling. The blade is made by bonding separate halves together at the shear webs and LE/TE regions. Each half is made in a female mould. The GRE girders are made first, and are then laid in the mould with the other

components (glass cloth and foam of appropriate thicknesses). The dry assembly is wrapped in vacuum bag material and a resin/hardener mixture is drawn through the components by vacuum pump. Once infusion is completed, the composite cures in the mould, with the vacuum bagging under pressure and with the assistance of heating. A schematic of the process is shown in Figure 4-12.

4.4.1.2 This method of manufacture is capable of producing reasonably consistent composites, in terms of porosity content and laminate thickness. It is generally more repeatable than wet lay-up, in which the glass cloth and resin are laid within a mould and cured without vacuum or heat. However, RIFT results in lower quality composites than the pre-preg method, in which glass cloth is pre-impregnated with resin prior to lay-up and cure.

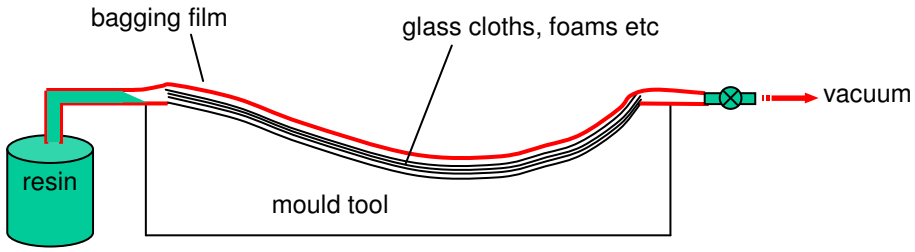

Figure 4-12 The RIFT process

4.4.1.3 It was planned that NOI Scotland staff would produce the RAM test panels during the latter stages of this project. However, they ceased trading during the final quarter. It was agreed with the DTI that the RAM test panels would be produced by QinetiQ, using nominally the same method and, where possible, the same materials. Some difficulties were experienced with the resin hardener, due to the fact that it is optimised for infusing large blade sections and not for making small test panels. An alternative hardener was procured that allowed the test panels to be produced to an acceptable standard.

4.4.2 Range of RAM panels produced

4.4.2.1 The variety of material thicknesses found along the NOI 34m blade has already been described (Section 4.1). It is possible to position a glass cloth lossy layer within a section of foam without mechanical detriment. This can be used, for example, to create a 10mm thick RAM within a 20mm thick foam sandwich panel. It was not necessary, therefore, to produce RAM variants for every foam thickness – especially in the time constraints imposed by the withdrawal of NOI from the project. The philosophy was to demonstrate a good RAM performance at each threat frequency band (i.e. ATC, weather and marine radar bands) for the thinnest foam possible, knowing that thicker sandwich panels could be made by combination with additional foam. Table 4-1 shows the full list of RAM variants produced.

	GRE/foam sandwich panels				GRE solid laminate
	5mm	10mm	15mm	20mm	
ATC		✓	✓	✓	
Weather		✓			✓
Marine	✓			✓	✓

Table 4-1 RAM panels produced

4.4.2.2 The NOI blade sandwich panels comprise contour core foam (sectioned foam on a carrier scrim, such that the foam can drape to the contours of the blade profile) between GRE skins containing 1200 $g.m^{-2}$ weight woven glass cloth. The lossy layers were modified 184 $g.m^{-2}$ plain weave glass cloths, treated with amino silane sizing agent to facilitate keying with the epoxy resin. The thickness of the cured lossy layer plus the 1200 $g.m^{-2}$ cloth was approximately 0.95mm, an increase of 0.18mm over the standard NOI GRE. A thinner version of the NOI glass cloth could be used in practice, in order to maintain the weight and thickness balance of the composite, but it was not feasible to obtain this in time for the panel manufacturing.

4.4.3 Microwave measurements

4.4.3.1 The microwave absorption performance of RAM panels was measured using either of two systems, depending on the frequency of interest. A free-space quasi-optical system, hereafter called the 'focussed horn system', was used for weather and marine frequencies. A schematic of this system is shown in Figure 4-13. Microwave signals are emitted from a pair of waveguide horn antennas, and the signals are brought to a focus at a common focal plane by parabolic mirrors. The system is calibrated using open circuit, short circuit and offset short circuit measurements, such that the focal plane becomes the phase reference for measurements. The material under test is positioned within an aperture at the focal plane, and the antennas are used to measure forward and reverse transmission and reflection coefficients, in magnitude and phase. The system operates from 5.2 GHz up to 18 GHz in 3 bands dictated by the cut-off frequencies of the waveguide antennas. Lower frequencies than 5.2 GHz cannot be measured due to the finite size of the mirrors. The focussing nature of the system means that samples need only be 350x350mm in size, for all bands.

4.4.3.2 Measurements of ATC panels were performed using a modified NRL arch arrangement in an anechoic chamber, using a pair of waveguide horn antennas of the appropriate band. The long wavelengths involved (100mm at 3 GHz, compared to 33mm at marine radar frequencies) result in the need for larger samples than for the focussed horn measurements. Typical samples were approximately 1m x 1m in size. A schematic of the system is shown in Figure 4-14. Calibration was made using a short circuit standard of

the same size as the material under test. The effect of multiple bounces and any interference from the supporting structure was removed using time-domain gating.

4.4.4 Results

4.4.4.1 The results for the ATC sandwich panels are show in Figures 4-15 to 4-17, for 10mm, 15mm and 20mm foam, respectively. The panels were also measured at higher frequencies using the focussed horn system, for completeness. The aim for these panels was to achieve performance within the 2.5 – 3 GHz frequency region, rather than for all panels to absorb at the same precise frequency. The latter could undoubtedly be achieved, but would have required a degree of tuning (in terms of glass cloth materials used, as well as lossy layer impedance) inappropriate for the budget of this project. Nevertheless, it can be seen that the materials achieve 25dB of absorption or better in the required band. This is seen as extremely encouraging, and there is no reason why the performance of the 20mm case (30dB absorption) could not be repeated for all of the foam thicknesses, given more effort. The solid GRE laminate panel was not made in the usual way, because the wet cloth laying machine used by NOI Scotland was not available and QinetiQ did not have a suitable similar machine available. An attempt was made to produce a 1m x 1m ATC panel by the RIFT method, but problems were encountered during manufacture and the resin did not infuse correctly. There was insufficient cloth and resin remaining to allow a further panel to be made in the available time, without precluding some of the other RAM panels being made. The solid GRE case is less important in any event, as the thickness available for introducing a RAM is more than adequate to create a RAM at ATC frequencies. It was decided that the sandwich panels were more challenging and that the remaining cloth and resin should be used for those cases.

4.4.4.2 The weather radar RAM panels were restricted to the 10mm foam and solid GRE cases. The performance of the 10mm foam RAM is shown in Figure 4-18, from both focussed horn and NRL arch systems. More than 30dB of absorption has been achieved in the region of 5.6 GHz, corresponding to a reflectivity of <0.1%. Thicker foam sandwich panels could be realised by adding more foam behind the carbon reflector of the RAM.

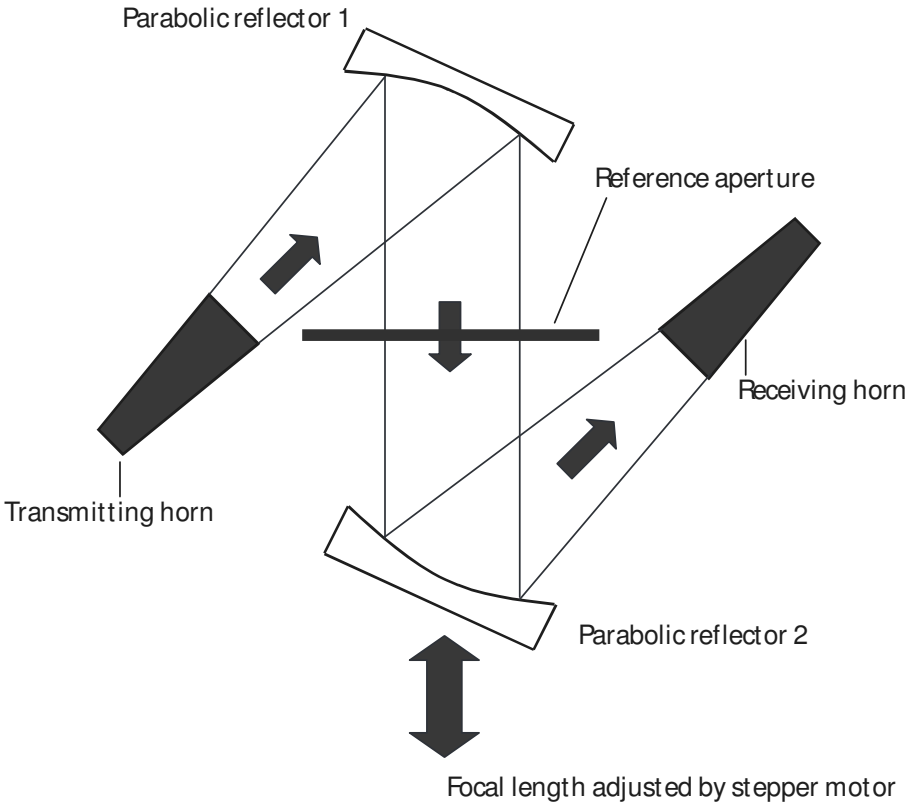

Figure 4-13 Focussed horn measurement system (>5GHz)

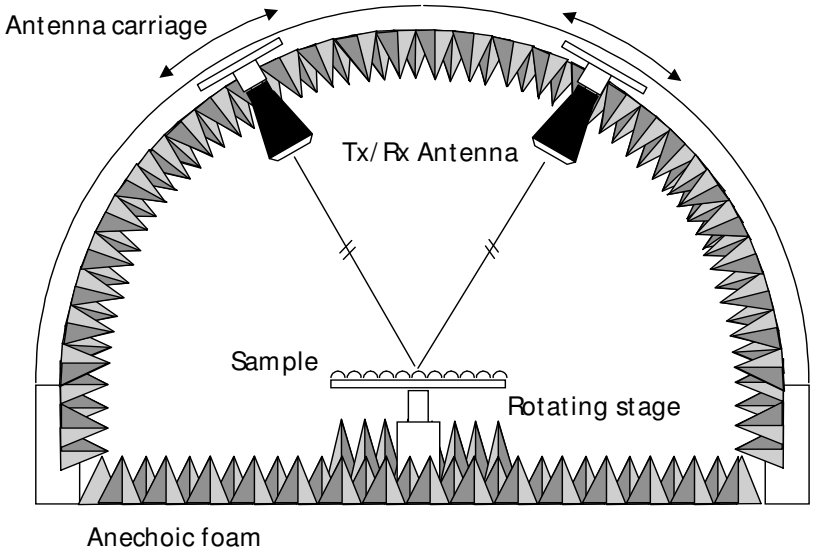

Figure 4-14 NRL arch measurement system (>2GHz)

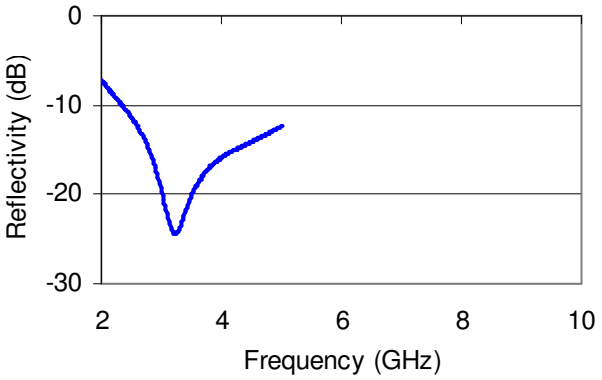

Figure 4-15 10mm foam sandwich panel RAM (ATC)

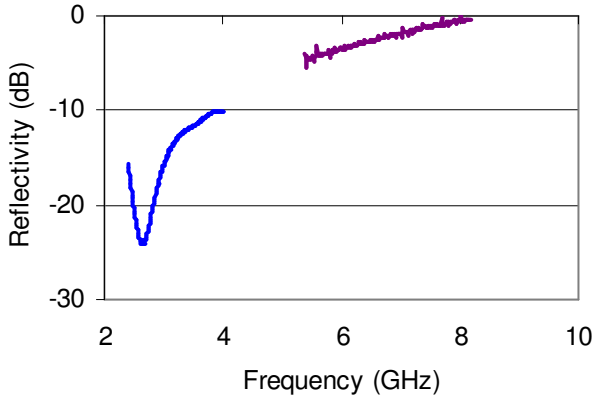

Figure 4-16 15mm foam sandwich panel RAM (ATC)

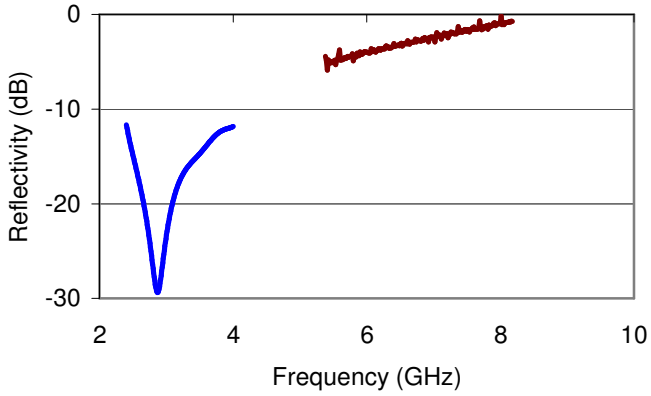

Figure 4-17 20mm foam sandwich panel RAM (ATC)

4.4.4.3 The measured performance of the solid GRE panel (weather) is shown in Figure 4-19. This exhibits 30dB of absorption at 5.6 GHz, which is in excess of the value used to calculate RCS and subsequent detection probability by weather radar.

4.4.4.4 The performances of the marine radar case RAMs are shown in Figures 4-20 to 4-22 for solid GRE and for 5mm foam and 20mm foam sandwich panels, respectively. All of these materials exhibit at least 20dB absorption performance, however this could be improved further if necessary, but such optimisation was beyond the scope of this project.

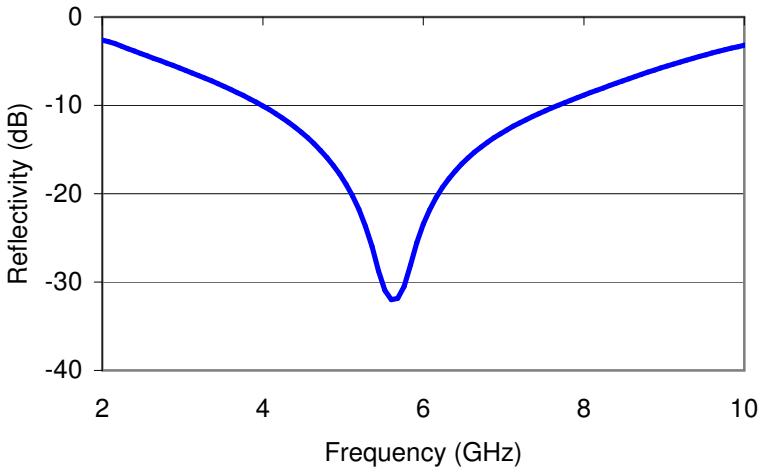

Figure 4-18 10mm foam sandwich panel RAM (Weather)

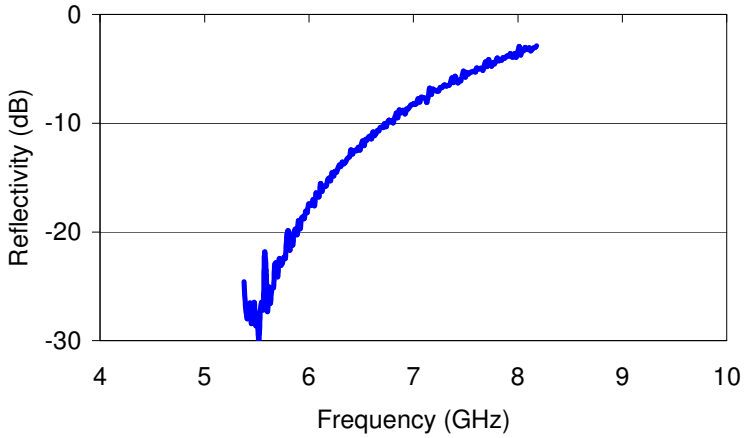

Figure 4-19 GRE RAM (Weather)

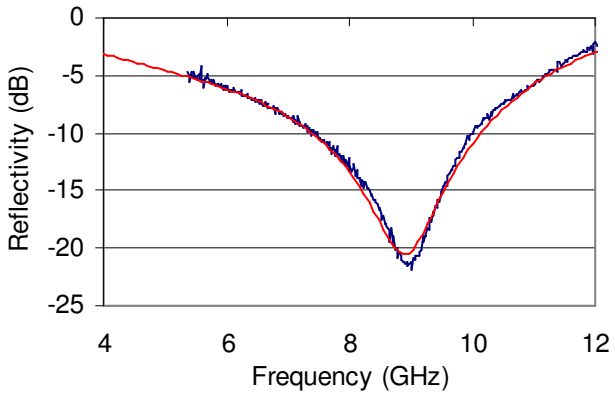

Figure 4-20 GRE RAM (Marine)

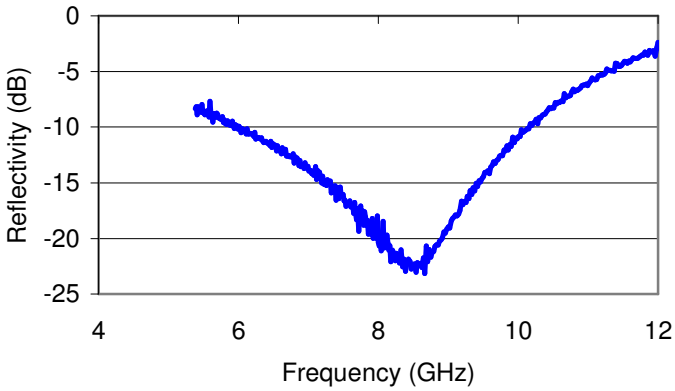

Figure 4-21 5mm foam sandwich panel RAM (Marine)

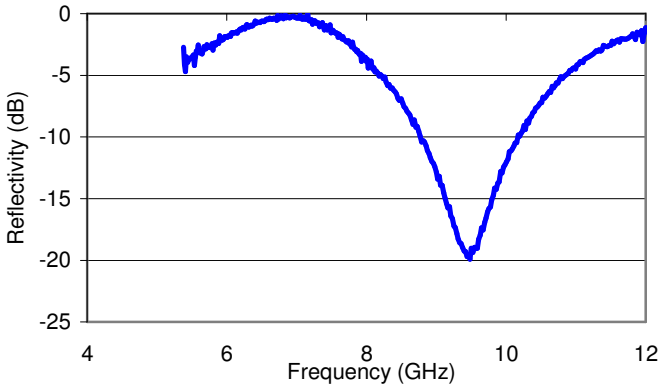

Figure 4-22 20mm foam sandwich panel RAM (marine)

5 CONCLUSIONS & RECOMMENDATION

5.1 RCS predictions

5.1.1 A CAD model of a typical wind turbine has been constructed using an NOI blade design. This has been used to calculate the likely radar cross section of a turbine with and without RAM treatments, as viewed by typical ATC, marine and weather radars over a range of blade yaw angles.

5.1.2 The calculations show that treating the blades with RAM leads to significant reductions in the peak RCS, although the median RCS level remains unaltered and the peak RCS remains high enough to allow detection by ATC radar. Treatment of the entire turbine with RAM leads to a reduction in both peak and median RCS, to a degree where the turbine's RCS is smaller than that of a typical small aircraft.

5.2 Radar Impact Modelling

5.2.1 A subset of predicted RCS values, including median and peak RCS values for untreated and RAM-treated turbines, has been used as input to the NEMESiS radar propagation model. The probability of detection of a wind turbine having the predicted RCS levels and being situated at a littoral site and an inland site in hilly terrain has been calculated for several turbine orientations and RCS configurations.

5.2.2 The impact of RCS reduction on the detection of the turbine by radar systems was calculated for cases where the whole turbine was treated with RAM. Although a modest decrease in the maximum detection range was found for weather radar (as is expected for such relatively powerful systems), much more significant reductions were predicted for ATC and marine radars. In the case of a turbine situated at the Hare Hill wind farm site near Ayr in Scotland, it was predicted that the turbine would be undetected for the majority of blade orientations by the ATC radar at nearby Prestwick airport.

5.3 Design of RAM blades

5.3.1 The various material compositions that exist on the NOI blade were studied and methods by which radar absorbent material (RAM) could be introduced to each region were identified. Materials present include solid glass fibre-reinforced epoxy (GRE) and GRE-skinned foam sandwich panels of a range of thicknesses. Materials samples were supplied by NOI and their microwave properties were measured and then used as input to RAM design codes that have been developed by QinetiQ and validated over many years. RAM designs have been sought that minimise the risk of any reduction in structural integrity of the blade.

5.3.2 It is possible to modify the solid GRE and GRE/foam sandwich panel materials used in the NOI 34m blade to create RAM, through the replacement of a single layer of glass cloth by an electromagnetically modified version of the same material. Absorption in the range 20dB to 30dB (i.e. reflected power is < 1%) can be readily achieved, even at the low frequencies (and hence large wavelengths) used by ATC radars. Performance of >25dB was achieved for most materials, though such fine-tuning for every material type was not considered necessary, as the main aim was to show proof-of-concept. This RAM approach is known to result in little or no degradation in the structural integrity of the blade materials, is compatible with the manufacturing processes used by NOI (and by most other blade manufacturers) and can be achieved at acceptable cost.

5.4 Recommendations

5.4.1 In summary, the study has shown that it is possible to modify all materials regions of the NOI 34m blade to create RAM, and that this can be done by methods which are known (from previous MoD-funded research on composite absorbers) to cause little or no degradation in structural properties. The predicted benefits in terms of reduced detection by non-Doppler radar and ATC radars are seen to be extremely encouraging.

5.4.2 However, predictive models can never fully represent reality, and there are factors that are difficult to accurately model, such as blade twist and bend. In light of this, it is recommended that a full practical demonstration of a stealthy turbine should be performed. All stakeholders (developers, manufacturers and planning objectors) will then be able to quantify the benefits of RCS reduction through the use of RAM.

REFERENCES

[1] Poupart, G.J., *Wind Farms Impact on Aviation Interests – Final Report*, QinetiQ, DTI PUB URN 03/1294, September 2003.

[2] C Anderson: "Blade shape and structural data NOI34-II". Cover letter to David Greenfield of QinetiQ dated September 22, 2003.

[3] Brewitt-Taylor, C.R., *Investigations of Possible Effects of Wind Turbines on Maritime Radio Frequency Systems*, QinetiQ/S&E/SPS/CR021315/1.0, July 2003.

[4] Butler, M.M. and D.A.Johnson, *Feasibility of Mitigating the Effects of Wind Farms on Primary Radar*, AMS, DTI PUB URN 03/976, 2003.

[5] Hopcroft, M.W., *Radar Impact Analysis for Gunfleet Sands Wind Farm*, QinetiQ/FST/CR023343/1.1, May 2002.

GLOSSARY OF TERMS

ATC	Air traffic control
CAD	Computer aided drawing
CFAR	Constant false alarm rate
FS	Foam sandwich
GHz	10^9 Hz
GRE	Glass fibre reinforced epoxy
LE	Leading edge
MTI	Moving target indicator
NEMESiS	Naval electromagnetic environment simulation suite
PEC	Perfect electrical conductor
RAM	Radar absorbent material
RCS	Radar cross section
RIFT	Resin infusion under flexible tolling
TE	Trailing edge